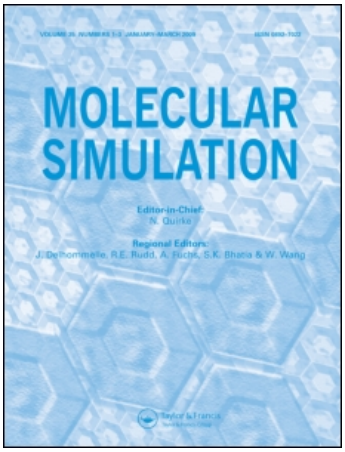

Molecular Simulation
Publication details, including instructions for authors and subscription information:
http://www.informaworld.com/smpp/title~content=t713644482

Molecular dynamics simulations of the interaction between polyhydroxylated compounds and Lennard-Jones walls: preferential affinity/exclusion effects and their relevance for bioprotection

Daan P. Geerke[a]; Wilfred F. van Gunsteren[a]; Philippe H. Hünenberger[a]
[a] Laboratory of Physical Chemistry, Swiss Federal Institute of Technology Zürich, Zürich, Switzerland

Online publication date: 16 August 2010

To cite this Article Geerke, Daan P. , van Gunsteren, Wilfred F. and Hünenberger, Philippe H.(2010) 'Molecular dynamics simulations of the interaction between polyhydroxylated compounds and Lennard-Jones walls: preferential affinity/exclusion effects and their relevance for bioprotection', Molecular Simulation, 36: 9, 708 — 728
To link to this Article: DOI: 10.1080/08927021003752804
URL: http://dx.doi.org/10.1080/08927021003752804

Molecular Simulation
Vol. 36, No. 9, August 2010, 708–728

Taylor & Francis
Taylor & Francis Group

Molecular dynamics simulations of the interaction between polyhydroxylated compounds and Lennard-Jones walls: preferential affinity/exclusion effects and their relevance for bioprotection

Daan P. Geerke[1], Wilfred F. van Gunsteren and Philippe H. Hünenberger*

Laboratory of Physical Chemistry, Swiss Federal Institute of Technology Zürich, ETH, CH-8093 Zürich, Switzerland

(*Received 1 October 2009; final version received 5 March 2010*)

Molecular dynamics simulation is used to investigate the interaction of methanol (MET) and the polyhydroxylated cosolutes (CSLs) ethylene glycol (ETG), glycerol (GLY), glucose (GLU) and trehalose (TRH) in aqueous solution with the surface of rigid Lennard-Jones walls. The walls are designed to represent simplified models for biomolecular (membrane, protein) surfaces and include three functionalisation variants: (i) non-polar (NP, no functionalisation); (ii) semi-polar (SP, surface hydroxyl groups); and (iii) highly polar (HP, positive and negative surface charges). The simulations are performed to investigate, in a simplified context, the preferential affinity/exclusion properties of the different CSLs (compared to water), which are relevant for the phenomenon of bioprotection by polyhydroxylated compounds. The simulations are carried out at three different temperatures (300, 475 and 600 K), and a comparison with simulations involving pure water or the pure liquid CSLs MET, ETG and GLY is also undertaken. In aqueous solution, all CSLs considered evidence preferential affinity (compared to water) for the NP and SP walls. This effect increases in magnitude with increasing CSL size, and is due to the favourable driving force associated with the replacement of multiple water molecules at the wall surface by a single polyhydroxylated CSL molecule (the partial substitution occurring without a significant change in the number of wall-solution hydrogen bonds). The preferential affinity is significantly reduced for the HP wall (for MET, ETG and GLY, preferential exclusion is actually observed). This change is probably related to the higher efficiency of water (compared to the CSLs) in terms of electrostatic solvation (higher dielectric permittivity), and provides an interpretation for the observation that polyhydroxylated CSLs appear to show preferential affinity for the surface of membranes, but preferential exclusion for the surface of proteins.

Keywords: molecular dynamics simulation; aqueous solutions; polyhydroxylated cosolutes; surface effects; preferential affinity or exclusion

1. Introduction

The cell membrane is the first component of a cell to interact with external solutes. The presence of cosolutes or cosolvents (CSLs) in the extracellular (aqueous) environment or in the intracellular medium can alter the physicochemical properties of this membrane, which may in turn affect the functioning of membrane proteins such as ion and water channels [1,2], or the resistance of the cell to potentially damaging conditions [3–5]. As a result, the modulation of membrane properties by CSLs and, in particular, by small mono- and polyhydroxylated compounds (both further collectively referred to as polyhydroxylated compounds for simplicity), is involved in several processes of high biological, technological and medicinal relevance [6]. Sugars play a central role in the ability of organisms to survive extreme conditions of dehydration, temperature, pressure, oxygen deprivation or salt concentration [3–5]. Alcohols or other small organic molecules are commonly used as anaesthetic agents [7–9]. Glycerol (GLY) and ethylene glycol (ETG) are frequently used as cryoprotective agents to minimise cellular damage in freezing technologies [10,11]. All these phenomena appear to involve, among other effects, a modulation of the properties of cell membranes by the CSL molecules [1–11].

The mechanisms whereby sugars stabilise membranes as well as other biomolecules under harsh conditions remain nowadays a matter of debate. In the case of dehydration resistance, three main hypotheses have been put forward. The water-replacement hypothesis suggests that sugars show preferential affinity (compared to water) for biomolecular surfaces [12–21], partially substituting water molecules in forming hydrogen bonds (H-bonds) with the polar and charged surface groups. In the case of lipid membranes, this H-bonded scaffold would be responsible for maintaining the spacing between the lipid headgroups and preserving the membrane in the liquid-crystalline phase throughout the dehydration–rehydration cycle [12,13,15,16]. In contrast, the water-entrapment hypothesis (mainly documented in the context of proteins [22,23], but also recently suggested in the context of membranes [24]) proposes that sugars are preferentially excluded (compared to water) from biomolecular surfaces

*Corresponding author. Email: phil@igc.phys.chem.ethz.ch

ISSN 0892-7022 print/ISSN 1029-0435 online

DOI: 10.1080/08927021003752804
http://www.informaworld.com

and, instead, concentrate residual water molecules close to the biomolecule. This residual water concentration would be responsible [25] for the preservation of the biomolecular solvation and native properties, even at very low water contents. Finally, the vitrification hypothesis suggests that sugars found in anhydrobiotic systems protect biomolecular structures through the formation of amorphous glasses, thereby reducing structural fluctuations and preventing mechanical disruption [26–31]. During the last few years, a combined view has also emerged that water replacement and vitrification might be simultaneously required to achieve bioprotection [3,4,14,21,30,32–36]. However, especially in the case of proteins [22,23,25,37–39], but also in the case of membranes [24,40,41], this view is not unanimously accepted.

Interestingly, computer simulation studies of proteins [42–47] and membranes [6,45,48–54] surrounded by aqueous sugar solutions have suggested different modes of interaction of sugars with the two types of biomolecular surfaces. While most protein simulations [42–47] showed preferential exclusion of the sugar molecules from the biomolecular surface (providing support to the water-entrapment hypothesis), most studies concerning membranes [6,45,48–54] showed preferential affinity of the sugar molecules for the biomolecular surface, with the partial replacement of water molecules in establishing H-bonds with the lipid headgroups (providing support to the water-replacement hypothesis).

This difference may tentatively be rationalised by considering the recent suggestion that the dielectric properties of the outer region of a water-soluble protein are nearly identical to those of its aqueous environment [55]. In contrast, the effective dielectric permittivity of the surface region of a membrane is typically assumed to be significantly lower than that of the solvent [56]. Although some care must be taken when interpreting estimates for local dielectric properties [57], it is probably reasonable to regard protein surfaces as being more polar than membrane surfaces, also when considering that the former surfaces present a significant density of side chains with net charges, while the latter ones typically embed neutral or zwitterionic headgroups. Accepting the existence of such a difference in surface polarity, one may relate observed dependencies of preferential affinity/exclusion effects to the composition (polarity) of the biomolecular surface.

In the case of membranes, the clustering of the sugar molecules at the membrane surface was also found in simulations to induce a marginal increase in the area per lipid and in the extent of disorder within the bilayer. The comparison of simulations involving different sugars did not reveal striking differences in their influence on the membrane properties [48,53]. However, the imposition of stress on the bilayer (e.g. elevated temperature or negative lateral pressure) was found to have a strong influence on the way sugar molecules interact with the lipid headgroups [49,53,54], as demonstrated by the observed increase in the number of sugar–lipid H-bonds and in the degree of bridging of the lipids via H-bonded sugar molecules.

The suggestion that the physiological effects of alcohols and other anaesthetics are (at least in part) due to the modulation of membrane properties is supported by the apparent lack of specific receptor sites for these molecules in the cell [58]. A non-specific interaction is also consistent, e.g. with the characteristics of ethanol intoxication, where a relatively high concentration is required to produce a response, above which the response is enhanced upon further increasing the concentration. However, the exact mode of action of alcohols (and other anaesthetic agents), as well as the hypotheses invoking lipids as the prime target in these processes, remain a matter of debate [58,59]. The interaction of alcohols with lipid membranes presents a peculiar characteristic, the so-called biphasic effect [60]. Depending on the concentration range, short-chain aliphatic alcohols have an opposite influence on the main gel-to-liquid-crystalline phase transition temperature T_m of membranes. At low concentrations, T_m decreases with increasing alcohol concentration, whereas at high concentrations, the opposite trend is observed. The biphasic effect was explained by the formation of an unusual interdigitated gel phase at high alcohol concentrations, where lipid molecules from the opposing monolayers interpenetrate [61]. The biphasic effect [60,61] as well as direct measurements [62–68] and computer simulations [6,69–74] of the influence of short-chain aliphatic alcohols on bilayer properties all suggest that these molecules show preferential affinity (compared to water) for the membrane surface. The intercalation of the alcohol molecules between the lipid headgroups [62–64,66] results in an increase in the effective headgroup volume, inducing a lateral expansion in the interfacial region [65,67,68]. When this expansion is important enough, the energetically unfavourable void spaces within the bilayer interior can be removed through interdigitation of the lipid tails [61–68,75–77]. Longer chain alcohols may induce a different response, presumably because their aliphatic chains are also able to intercalate between the lipid tails [78]. In line with the general tendency of alcohols to significantly increase the headgroup spacing, an increase in the disorder (decrease in the order parameters) of the lipid hydrocarbon tails is observed when alcohols are added to lipid bilayers in the liquid-crystalline phase [63,64,66] (provided that the system does not undergo transition to the interdigitated gel phase). This disorder increase is caused by a reduction in the packing constraints imposed on the lipid tails. Direct interactions between the alcohol molecules and the lipid headgroups have also been observed in simulations in the form of H-bonds between

the alcohol hydroxyl groups and both the phosphate and ester groups of the lipids [6,73,74], in agreement with experimental observations [65,66].

Similar to short-chain aliphatic alcohols, ETG and GLY can induce (at sufficiently high concentrations) the formation of interdigitated phases in phospholipid bilayers [79–82]. Multilamellar liposomes can be formed in pure GLY with similar properties (spacing between bilayers, main transition temperatures, heat capacities and enthalpies) to those formed in pure water (WAT) [79]. Such liposomes can also be formed in pure ETG [79]. ETG in aqueous solution has also been shown to present a biphasic effect [81] and to promote an increase in the disorder of the lipid tails [83,84] for bilayers in the liquid-crystalline phase. A number of studies have suggested that GLY interacts directly, through H-bonds, with the lipid headgroups [85,86]. However, a recent calorimetric investigation has concluded that GLY is preferentially excluded from the membrane–water interface [87], in apparent disagreement with the previous experimental studies. In the case of proteins embedded in aqueous GLY solutions, both preferential affinity [21] of the triol (compared to water) for the protein surface and preferential exclusion [88] of the triol (compared to water) from the protein surface have been suggested by independent experiments. To our knowledge, only a few simulation studies [6,89–91] have investigated the interaction of ETG and GLY with biomolecules. Two of these [6,90] indicated a preferential affinity of ETG or GLY for the surface of a membrane, whereas the third one [91] indicated a preferential exclusion of GLY from the surface of a protein.

In spite of numerous experimental and theoretical investigations (see above), a complete understanding of the molecular mechanisms responsible for the modulation of the properties of lipid bilayers and other biomolecules by polyhydroxylated CSLs is still lacking. In a previous theoretical study [6], we used molecular dynamics (MD) simulations to investigate in a systematic fashion the interaction of methanol (MET) and the polyhydroxylated CSLs ETG, GLY, glucose (β-D-glucopyranose, GLU) and trehalose (α,α-trehalose, TRH) with a hydrated dipalmitoylphosphatidylcholine (DPPC) bilayer in the liquid-crystalline phase at 325 K. The comparison was performed at constant effective concentration of CSL hydroxyl groups. The results, along with available experimental data, led to the formulation of two distinct mechanisms for the interaction of polyhydroxylated compounds with lipid bilayers: the alcohol-like mechanism and the sugar-like mechanism.

The alcohol-like mechanism (active for MET and ETG) involves preferential affinity of the CSL (compared to water) for the superficial region of the bilayer interior, and is driven by the hydrophobic effect. It results in a lateral expansion of the membrane, a disorder increase within the bilayer and a partial substitution of water by CSL molecules at the H-bonding sites provided by the membrane, predominantly at the level of the ester groups. The sugar-like mechanism (active for GLU and TRH) involves preferential affinity of the CSL (compared to water) for the bilayer surface (leading to the formation of a coating layer), and is driven by entropic effects. It results in the absence of significant lateral expansion and disorder increase within the bilayer, and in a partial substitution of water by CSL molecules at the H-bonding sites provided by the membrane, predominantly at the level of the phosphate groups. It also involves the bridging of lipid molecules via H-bonded CSL molecules, a phenomenon that may have implications in the context of membrane stabilisation by sugars [6]. Note that H-bonding itself is not viewed as a driving force for these two mechanisms [6], which only involve the (partial) substitution of water–lipid by CSL–lipid H-bonds, the sum of the two remaining essentially constant, irrespective of the nature and concentration of the CSL.

The goal of the present work is to provide further insight into the mechanism of interaction of polyhydroxylated CSLs with lipid bilayers in the context of simplified interface models. More specifically, the bilayer is replaced here by a rigid wall composed of a lattice of positionally constrained Lennard-Jones particles LJP. This wall may present either a non-polar (NP; unaltered LJPs), a semi-polar (SP; partial hydroxylation of the surface LJPs) or a highly polar (HP; partial ionisation of the surface LJPs) surface. It is exposed either to aqueous solutions of the different CSLs (MET, ETG, GLY, GLU or TRH), to the different pure liquid CSLs (MET, ETG and GLY only) or to WAT. In the case of aqueous CSL solutions, the comparison is performed at constant effective CSL oxygen atom concentration. This permits to investigate specifically the effect of the configurational (geometrical and stereochemical) restrictions imposed by a given molecular framework on the capacity of the CSL H-bonding groups to interact with the wall. Note that this choice differs slightly from the one used in our previous work on CSL–membrane interactions [6] (constant effective CSL hydroxyl group concentration) because, unlike the headgroups of a DPPC bilayer, the functionalised LJPs in the surface layers of the SP wall can function not only as H-bond acceptors but also as H-bond donors. Explicit-solvent MD simulations of these systems on the nanosecond time scale are performed at constant volume and at three different temperatures (300, 475 or 600 K). Because the walls are fully rigid, precluding any lateral expansion, intercalation of the CSL molecules between the surface LJPs (mimicking the lipid headgroups) is nearly impossible. For this reason, the alcohol-like mechanism should be essentially inactive in these systems, thereby permitting a specific investigation of preferential affinity caused by the sugar-like (entropy-driven) mechanism. In addition, rigid walls present the advantage over more realistic phospholipid membranes that they do not undergo

slow internal processes, so that possible convergence problems are essentially eliminated in the present simulations.

2. Methods

2.1 MD simulations

All MD simulations were carried out using the GROMOS96 program [92,93]. The force-field parameters used in the present work were as follows: the SPC model of Berendsen et al. [94] was used for water; the B3 model of Walser et al. [95] for MET; the G04 model of Geerke and van Gunsteren [96] for ETG; the model of Geerke as reported by Pereira and Hünenberger [6] for GLY; and the GROMOS 45A4 force-field parameters of Lins and Hünenberger [97] for GLU and TRH. Although these force-field parameter sets have been developed by different authors, they all consistently follow the parameterisation philosophy underlying the GROMOS biomolecular force field [92,98], including compatibility with the SPC water model, i.e. they were calibrated against experiment to reproduce key thermodynamic properties of the pure substance and of its aqueous mixtures. The force-field parameters used for the LJPs of the walls (as well as the oxygen (OSP) and hydrogen (HSP) atoms of the surface hydroxyl groups for the SP walls) are provided in Table 1.

Three types of walls were considered, differing in their surface properties: a NP; a SP; and a HP wall. The three types of wall share a common basic framework consisting of seven layers (along the z-axis) of 16×16 LJPs (in the xy-plane), in a rigid cubic lattice with lattice spacing $r_{\mathrm{LJP-LJP}} = 0.21\,\mathrm{nm}$, resulting in a total wall dimension of $3.36 \times 3.36 \times 1.47\,\mathrm{nm}^3$. Note that a relatively high density of LJPs in the wall was selected, so as to prevent the penetration of the water molecules into the surface layers during the simulations. In the NP wall, all LJPs were assigned a zero charge, and no surface modification was applied. In the SP wall, one-half of the $2 \times 16 \times 16$ surface LJPs were functionalised by hydroxyl groups, alternating functionalised and unfunctionalised LJPs for closest neighbours. These hydroxyl groups are rigid and anchored to the wall such that the LJP—OSP bond is oriented perpendicularly to the surface layer (along the z-axis), i.e. they possess a single (dihedral angle) degree of freedom. The selected spacing between the hydroxyl groups of the SP wall (0.297 nm between nearest-neighbour hydroxyl oxygen atoms) is similar to the corresponding nearest-neighbour distance in pure WAT (0.278 nm) [99] and pure MET (0.275 nm) [100]. In the HP wall, one-half of the $2 \times 16 \times 16$ surface LJPs were assigned a net charge of $+1e$ or $-1e$, alternating charged and uncharged LJPs for closest neighbours, and positive and negative charges for closest charged neighbours.

The simulations were performed under periodic boundary conditions (at constant volume), based on reference boxes of dimensions $L_x \times L_y \times L_z$ with $L_x = L_y = 3.36\,\mathrm{nm}$, containing one copy of the above wall (now becoming a set of parallel walls periodic along the z-axis, each of which being of infinite extent in the x- and y-directions) along with either an aqueous CSL solution, a pure liquid CSL (MET, ETG and GLY only), or pure WAT. The composition of these systems and the corresponding L_z values are reported in Table 2 for the different systems. The values of L_z were chosen in such a way that the approximate solution volume is equal to the average volume obtained from an independent constant pressure simulation of the corresponding aqueous mixture or pure liquid in the absence of the Lennard-Jones wall (note that L_z is slightly larger for the SP wall, to account for the extra volume occupied by the additional hydroxyl groups at the surface). The CSL and/or water molecules were initially placed at random positions and with random orientations in the reference box, in such a way that they were not overlapping with each other or with wall particles.

Table 1. Force-field parameters used for the LJPs of the walls, as well as for the OSP oxygen and HSP hydrogen atoms of the surface hydroxyl groups for the SP wall.

Particle	Parameter	Value	Units
LJP	$C_6^{1/2}$	0.09805	$(\mathrm{kJ\,mol^{-1}\,nm^6})^{1/2}$
	$C_{12}^{1/2}$	5.162	$10^{-3}\,(\mathrm{kJ\,mol^{-1}\,nm^{12}})^{1/2}$
	q	0.000[a]	e
		0.266[b]	e
		± 1.0[c]	e
	$r_{\mathrm{LJP-LJP}}$	0.21	nm
OSP	$C_6^{1/2}$	0.04756	$(\mathrm{kJ\,mol^{-1}\,nm^6})^{1/2}$
	$C_{12}^{1/2}$	1.100[d]	$10^{-3}\,(\mathrm{kJ\,mol^{-1}\,nm^{12}})^{1/2}$
		1.227[e]	$10^{-3}\,(\mathrm{kJ\,mol^{-1}\,nm^{12}})^{1/2}$
	q	-0.674	e
	$r_{\mathrm{LJP-OSP}}$	0.143	nm
HSP	$C_6^{1/2}$	0.000	$(\mathrm{kJ\,mol^{-1}\,nm^6})^{1/2}$
	$C_{12}^{1/2}$	0.000	$10^{-3}\,(\mathrm{kJ\,mol^{-1}\,nm^{12}})^{1/2}$
	q	0.408	e
	$r_{\mathrm{OSP-HSP}}$	0.100	nm
	$r_{\mathrm{LJP-HSP}}$	0.1988	nm

Notes: The parameters listed are the square-root Lennard-Jones coefficients ($C_6^{1/2}$ and $C_{12}^{1/2}$, to be used with a geometric-mean combination rule [92]), the atomic partial charges (q) and the (constrained) distance between two bonded atoms of a given type i and j (r_{i-j}). The walls are composed of seven layers (along the z-axis) of 16×16 LJPs (in the xy-plane) in a rigid cubic lattice with lattice spacing $r_{\mathrm{LJP-LJP}}$. For the NP wall, all LJPs are unfunctionalised and uncharged. For the SP wall, one-half of the $2 \times 16 \times 16$ surface LJPs are functionalised by OSP–HSP hydroxyl groups (alternating functionalised and unfunctionalised LJPs; rigid bond distances and bond angles, orientation of the LJP—OSP bond constrained to be perpendicular to the wall surface; only one freely rotating dihedral angle). For the HP wall, one-half of the $2 \times 16 \times 16$ surface LJPs are charged (alternating charged and uncharged LJPs for closest neighbours, and positive and negative charges for closest charged neighbours). All atoms (LJP, OSP and HSP) within a wall are excluded from Lennard-Jones interactions with each other. Note also that hydrogen atoms (wall and system) are not involved in van der Waals interactions. [a] NP, SP and HP walls except surface layers. [b] SP wall surface layers (functionalised LJP only). [c] HP wall surface layers (charged LJP only). [d] For interactions between OSP and carbon atoms in the system. [e] For interactions between OSP and oxygen atoms in the system.

Table 2. Composition of the simulated systems (reference box).

System	n_O	N_{CSL}	N_{WAT}	m_{CSL} (mol kg^{-1})	m_O (mol kg^{-1})	NP, HP walls		SP wall	
						L_z (nm)	l_z (nm)	L_z (nm)	l_z (nm)
Aqueous CSL									
MET	1	300	1400	11.89	11.89	7.5446	1.83	7.6610	1.92
ETG	2	150	1400	5.947	11.89	7.0376	1.83	7.1540	1.92
GLY	3	100	1400	3.965	11.89	6.8896	1.83	6.8970	1.92
GLU	6	50	1400	1.982	11.89	6.7806	1.83	6.7704	1.92
TRH	12	25	1400	0.991	11.89	6.6540	1.83	6.8970	1.92
Pure CSL									
MET	1	925				7.5446	1.83	7.6610	1.92
ETG	2	609				7.0376	1.83	7.1540	1.92
GLY	3	452				6.8896	1.83	6.8970	1.92
Pure water									
WAT	1	1748				6.7806	1.83	6.7704	1.92

Notes: The parameters listed are the number of oxygen atoms per CSL molecule (n_O), the number of CSL (N_{CSL}) and water (N_{WAT}) molecules in the box, the solution molality m_{CSL} (number of moles of CSL divided by the mass of water), the effective CSL oxygen atom molality m_O ($= m_{CSL} \times n_O$), and the box length L_z and estimated wall thickness l_z in the z-direction (perpendicular to the wall). The different entries correspond to aqueous solutions of the CSLs MET, ETG, GLY, GLU or TRH, to the pure CSL liquids (MET, ETG and GLY only) or to WAT, in the vicinity of either a NP, a SP or a HP wall.

In all subsequent energy minimisations and MD simulations, the LJPs and, in the case of the SP wall, the OSPs were positionally constrained. The simulations were performed at constant volume and at three different temperatures of 300, 475 or 600 K. After a steepest-descent energy minimisation, initial velocities were assigned from a Maxwell–Boltzmann distribution at the appropriate temperature. After an equilibration period of 10^7 MD steps, production runs of 5×10^6 steps were carried out, in which data for analysis (energies, atomic coordinates) were written to file every 5000 steps.

All MD simulations relied on integrating Newton's equations of motion based on the leap-frog algorithm [101], with time steps of 2, 1.5 and 1.4 fs, at 300, 475 and 600 K, respectively (leading to production runs of 10, 7.5 and 7 ns, respectively). The temperature was maintained at the appropriate average value using the weak-coupling method of Berendsen et al. [102] (with a coupling time of 0.1 ps). In the case of the aqueous CSL solutions, the degrees of freedom of the CSL and water molecules were coupled to two separate baths. Bond lengths were constrained to their minimum energy values using the SHAKE algorithm [103] with a relative geometric tolerance of 10^{-4}. Non-bonded interactions were handled using a twin-range cut-off scheme [104]. Within a short-range cut-off radius of 0.8 nm, interactions were evaluated every time step based on a pairlist that was updated every five steps. The intermediate-range interactions up to a long-range cut-off radius of 1.4 nm were evaluated simultaneously with each pairlist update, and assumed constant in between. To account for the mean effect of electrostatic interactions beyond the long-range cut-off radius, a reaction-field correction [105] was applied using an effective relative dielectric permittivity of 50.

2.2 Analysis

The analysis was performed in terms of: (i) the normalised probability distribution function $p_\alpha(z)$ of species α (CSL or WAT) along the direction normal to the wall (z-axis); (ii) the excess surface fraction $f_\alpha(d_c)$ of species α within a cut-off distance d_c from the wall surface; (iii) estimates for the standard (Helmholtz) free energy ΔA°_α, energy ΔU°_α and entropy ΔS°_α associated with the bulk-to-surface equilibrium for species α (for a selected value of d_c; aqueous CSL solutions only); (iv) H-bonding between species α and the wall (SP wall only); and (v) orientational preferences of the CSL molecules close to the wall (aqueous CSL solutions only). For the CSLs, quantities (i)–(iii) represent averages over all carbon atoms of the molecule. For WAT, these quantities refer to the oxygen atom of the water molecule.

The normalised probability distribution $p_\alpha(z)$ of a species α along the z-axis was evaluated according to

$$p_\alpha(z) = \frac{L_z - l_z}{N_\alpha} \sum_{i=1}^{N_\alpha} \langle \delta(z_i(t) - z) \rangle_t, \qquad (1)$$

where N_α is the total number of sites allocated to species α (CSL, all carbon atoms; WAT, oxygen atom) in the computational box; L_z is the box size along the z-axis; and l_z is the estimated wall thickness along the z-axis (Table 2). In this equation, the function $z_i(t)$ represents the z-coordinate of the ith site at time t; δ is the Dirac delta function; and $< \cdots >_t$ denotes (infinite) ensemble (time) averaging. The value of $z_i(t)$ was selected within a period L_z, such that $z = 0$ and $z = L_z$ correspond to the middle planes of a wall and of its next (parallel) periodic image along the z-axis, respectively. Because $p_\alpha(z)$ essentially vanishes for z in the intervals $[0, \frac{1}{2} l_z]$ and $[L_z - \frac{1}{2} l_z, L_z]$, this function is normalised to an (approximate) average value

of 1 over the interval $[\frac{1}{2}l_z, L_z - \frac{1}{2}l_z]$, i.e.

$$\frac{1}{L_z - l_z}\int_{\frac{1}{2}l_z}^{L_z-\frac{1}{2}l_z} p_\alpha(z)\,\mathrm{d}z \approx \frac{1}{L_z - l_z}\int_0^{L_z} p_\alpha(z)\,\mathrm{d}z = 1. \quad (2)$$

This choice of normalisation, although slightly approximate, was made because it should lead to profiles independent of the wall thickness (for large enough l_z) and surface characteristics independent of the solution volume (for large enough $L_z - l_z$). In practice, the δ-function in Equation (1) was approximated by a binning function of width $\Delta z = 0.02$ nm and the infinite ensemble (time) average replaced by a (finite and discrete) trajectory average over the entire production time, leading to a corresponding histogram approximation for $p_\alpha(z)$. The value of l_z was set to 1.83 nm for the NP and HP walls, and to 1.92 nm for the SP wall (Table 2). These were estimated empirically as optimal compromise values for the different systems, types of sites and temperatures from the zero point of the density profiles. Deviations from these compromise values were always below 0.09 nm and can be neglected.

For the description of excess surface properties, it is convenient to introduce the notations bulk(d_c) for the interval $[\frac{1}{2}L_z - \frac{1}{2}d_c, \frac{1}{2}L_z + \frac{1}{2}d_c]$ and surf(d_c) for the union of the intervals $[\frac{1}{2}l_z, \frac{1}{2}l_z + d_c]$ and $[L_z - (\frac{1}{2}l_z + d_c), L_z - \frac{1}{2}l_z]$. To determine the excess surface fraction $f_\alpha(d_c)$ of species α for a given cut-off distance d_c from the wall surface, the average numbers of particles $n_{\alpha,\mathrm{surf}}(d_c)$ within surf(d_c) and $n_{\alpha,\mathrm{bulk}}(d_c)$ within bulk(d_c) were calculated according to

$$n_{\alpha,\mathrm{surf}}(d_c) = \frac{N_\alpha}{L_z - l_z}\int_{\mathrm{surf}(d_c)} p_\alpha(z)\,\mathrm{d}z \quad (3)$$

and

$$n_{\alpha,\mathrm{bulk}}(d_c) = \frac{N_\alpha}{L_z - l_z}\int_{\mathrm{bulk}(d_c)} p_\alpha(z)\,\mathrm{d}z. \quad (4)$$

The excess surface fraction $f_\alpha(d_c)$ of species α was then calculated according to

$$f_\alpha(d_c) = \frac{n_{\alpha,\mathrm{surf}}(d_c) - 2n_{\alpha,\mathrm{bulk}}(d_c)}{n_{\alpha,\mathrm{surf}}(d_c) + 2n_{\alpha,\mathrm{bulk}}(d_c)}. \quad (5)$$

Three limiting cases for $f_\alpha(d_c)$ are: (i) full exclusion from the wall ($p_\alpha(z) = 0$ over surf(d_c)); (ii) inert behaviour relative to the wall ($p_\alpha(z) = 1$ over surf(d_c) and bulk(d_c)); and (iii) full affinity to the wall ($p_\alpha(z) = 0$ over bulk(d_c)). In these cases, one has

$$f_\alpha(d_c) = \begin{cases} -1 & \text{full exclusion} \\ 0 & \text{inert behaviour} \\ 1 & \text{full affinity.} \end{cases} \quad (6)$$

The standard (Helmholtz) free energy ΔA°_α associated with the bulk-to-surface equilibrium for species α was estimated by assuming a two-state process (based on a selected value for the cut-off distance d_c from the wall surface; aqueous CSL solutions only). Because the solutions considered are relatively concentrated and because it was convenient to treat CSL and WAT on the same footing, a reference state based on mole fractions x_α (rather than molalities m_α, more commonly used in solution chemistry) was adopted. In this case, ΔA°_α is defined as the free energy for transferring 1 mole of species α from a bulk solution at infinite dilution to the surface region at infinite dilution, extrapolated to a reference mole fraction $x_\alpha = 1$ in both regions assuming ideal solution behaviour. Assuming that ideal solution behaviour approximately holds in the finite concentration regime considered in the simulations, one may write for the chemical potential μ_α in the two regions

$$\mu_{\alpha,\mathrm{bulk}} = \mu^\circ_{\alpha,\mathrm{bulk}} + RT\ln x_{\alpha,\mathrm{bulk}} \quad (7)$$

and

$$\mu_{\alpha,\mathrm{surf}} = \mu^\circ_{\alpha,\mathrm{surf}} + RT\ln x_{\alpha,\mathrm{surf}}. \quad (8)$$

At equilibrium (simulation conditions), one should have

$$\mu_{\alpha,\mathrm{bulk}} = \mu_{\alpha,\mathrm{surf}}, \quad (9)$$

so that

$$\Delta A^\circ_\alpha = \mu^\circ_{\alpha,\mathrm{surf}} - \mu^\circ_{\alpha,\mathrm{bulk}} = RT\ln\frac{x_{\alpha,\mathrm{bulk}}}{x_{\alpha,\mathrm{surf}}}. \quad (10)$$

The involved ratio can be calculated as (for a given d_c)

$$\frac{x_{\alpha,\mathrm{bulk}}}{x_{\alpha,\mathrm{surf}}} = \frac{\int_{\mathrm{bulk}(d_c)}\mathrm{d}z\,p_\alpha(z)}{\int_{\mathrm{bulk}(d_c)}\mathrm{d}z\,[p_{\mathrm{CSL}}(z) + p_{\mathrm{WAT}}(z)]} \times \frac{\int_{\mathrm{surf}(d_c)}\mathrm{d}z[p_{\mathrm{CSL}}(z) + p_{\mathrm{WAT}}(z)]}{\int_{\mathrm{surf}(d_c)}\mathrm{d}z\,p_\alpha(z)}. \quad (11)$$

The corresponding entropy change ΔS°_α (at constant number of particles and volume) can be estimated through values of ΔA°_α at two different temperatures as

$$\Delta S^\circ_\alpha(T) \approx -\frac{\Delta A^\circ_\alpha(T + \frac{1}{2}\Delta T) - \Delta A^\circ_\alpha(T - \frac{1}{2}\Delta T)}{\Delta T} \quad (12)$$

and the corresponding internal energy ΔU°_α (at constant number of particles and temperature) through the Gibbs equation as

$$\Delta U^\circ_\alpha = \Delta A^\circ_\alpha + T\Delta S^\circ_\alpha. \quad (13)$$

In principle, because a two-state equilibrium is considered, the values of ΔA°_α (as well as ΔS°_α and ΔU°_α) calculated

in this way should be unaltered if the standard state is changed to the (more common) reference state based on a solution of unit molality (although the corresponding values of $\mathring{\mu}_{\mathrm{CSL,bulk}}$ and $\mathring{\mu}_{\mathrm{CSL,surf}}$ would be). Note that the calculation assumes ideal-mixture behaviour, so that the resulting values should be regarded as crude estimates (especially at high CSL concentrations). A more accurate determination would require complementary investigations in the dilute regime.

Another quantity of interest is the free energy change $\Delta_{\mathrm{exc}}\mathring{A}_{\mathrm{CSL}}$ associated with the exchange reaction

$$1\,\mathrm{CSL\,(bulk)} + n_{\mathrm{O}}\,\mathrm{WAT\,(surf)} \rightarrow 1\,\mathrm{CSL\,(surf)} + n_{\mathrm{O}}\,\mathrm{WAT\,(bulk)}, \quad (14)$$

where n_{O} is the number of oxygen atoms in a single CSL molecule (Table 2). This quantity can be easily calculated as

$$\Delta_{\mathrm{exc}}\mathring{A}_{\mathrm{CSL}} = \Delta\mathring{A}_{\mathrm{CSL}} - n_{\mathrm{O}}\Delta\mathring{A}_{\mathrm{WAT}}. \quad (15)$$

Similar equations also hold for the corresponding entropic and energetic contributions $\Delta_{\mathrm{exc}}\mathring{S}_{\mathrm{CSL}}$ and $\Delta_{\mathrm{exc}}\mathring{U}_{\mathrm{CSL}}$.

The average number of H-bonds formed between the wall surface and the CSL or WAT molecules was monitored (SP wall only). A H-bond was assumed to be present for a hydrogen–acceptor distance smaller than 0.3 nm and a donor–hydrogen–acceptor angle larger than 135°.

Finally, orientational preferences of the CSL molecules close to the wall were evaluated by monitoring distribution profiles (Equation (1)) separately for sites α corresponding to the carbon or oxygen atoms of the CSLs (aqueous CSL solutions only).

3. Results

The normalised probability distribution functions $p_\alpha(z)$ for the species α (CSL, all carbon atoms; WAT, oxygen atom; Equation (1)) in the simulations involving aqueous CSL solutions in the presence of the three types of wall (NP, SP and HP) are displayed in Figures 1–3 for the three temperatures considered (300, 475 and 600 K, respectively).

In most cases, the distribution profiles are, as expected, symmetrical relative to the point $z = L_z/2$, suggesting that the corresponding ensemble averages are converged. As an independent test for convergence, distribution profiles were also calculated separately for 10 successive trajectory blocks along the different simulations and, considering the final distributions that are symmetrical, no systematic differences or drifts in the curves were observed for the successive blocks (data not shown). However, for the simulations involving a HP wall, in particular at the two lowest temperatures and for the largest CSL molecules (the two sugars), a significant extent of asymmetry in the profiles (as well as a significant variability among the 10 block-averaged profiles) indicates an incomplete convergence of the simulations.

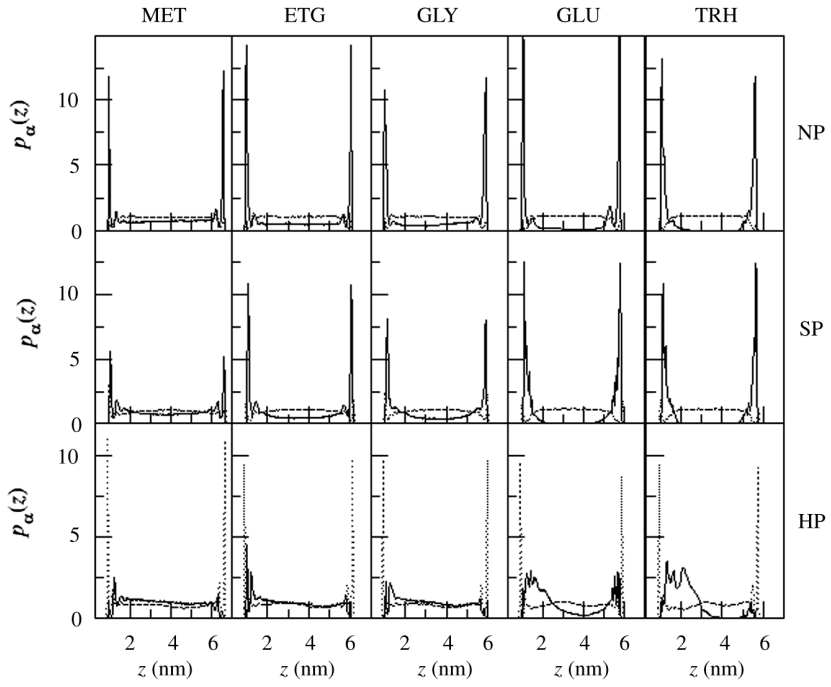

Figure 1. Normalised probability distribution functions $p_\alpha(z)$ (Equation (1)) at $T = 300$ K for the carbon atoms of the MET, ETG, GLY, GLU or TRH molecules (solid lines) and for the oxygen atom of the WAT molecules (dotted lines), corresponding to aqueous CSL solutions in the vicinity of a NP, SP or HP wall. The origin ($z = 0$) corresponds to the centre of the wall.

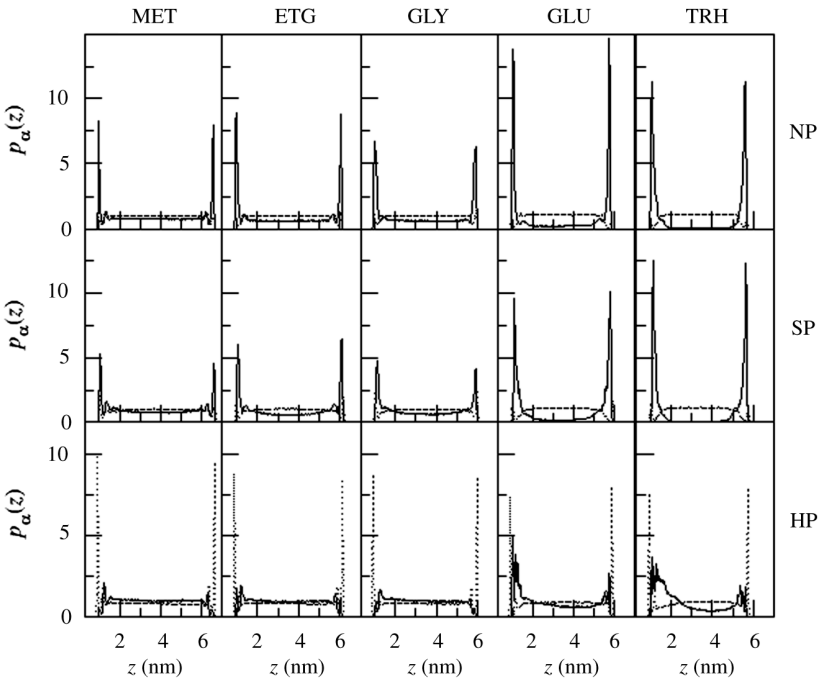

Figure 2. Normalised probability distribution functions $p_\alpha(z)$ (Equation (1)) at $T = 475$ K for the carbon atoms of the MET, ETG, GLY, GLU or TRH molecules (solid lines) and for the oxygen atom of the WAT molecules (dotted lines), corresponding to aqueous CSL solutions in the vicinity of a NP, SP or HP wall. The origin ($z = 0$) corresponds to the centre of the wall.

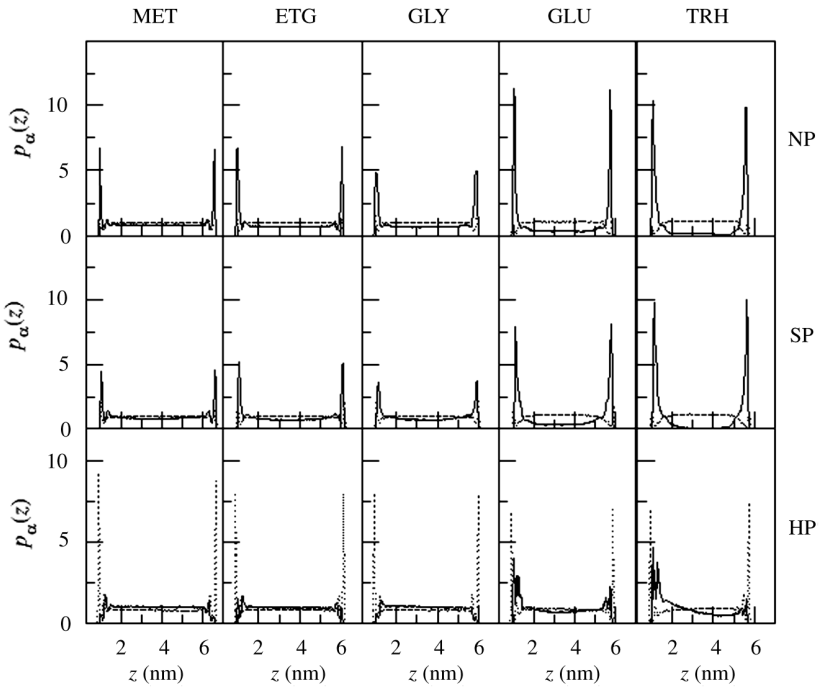

Figure 3. Normalised probability distribution functions $p_\alpha(z)$ (Equation (1)) at $T = 600$ K for the carbon atoms of the MET, ETG, GLY, GLU or TRH molecules (solid lines) and for the oxygen atom of the WAT molecules (dotted lines), corresponding to aqueous CSL solutions in the vicinity of a NP, SP or HP wall. The origin ($z = 0$) corresponds to the centre of the wall.

In the simulations at 300 K, the presence of the HP wall actually induces the appearance of empty spaces (bubbles) in the simulation box. This behaviour most likely results from very strong electrostatic interactions between the solution and the charged LJPs of the wall, inducing a transition to a glassy state. For these reasons, the results

of the simulations with the HP wall at 300 K are not considered further in this analysis. The corresponding results at 475 and 600 K are reported, but should be taken with some caution in the case of the sugar solutions considering the significant asymmetry of the $p_\alpha(z)$ profiles (Figures 2 and 3).

At the three temperatures, the considered polyhydroxylated CSLs systematically show an increased density (peaks around $z = l_z/2$ and $z = L_z - l_z/2$) at the surface of a NP or a SP wall, while WAT presents a decreased density (dips around $z = l_z/2$ and $z = L_z - l_z/2$). In other words, all CSLs show preferential affinity (relative to water) for the NP and SP walls, i.e. the solution in the surface region is more concentrated in CSL compared to the bulk. In some cases (especially for the smallest CSLs), multiple CSL density peaks (typically a higher first peak and a lower second peak) are observed close to the wall surface, revealing some layering effect. Preferential affinity appears to be particularly strong for the sugar CSLs. In this case, the concentration of sugar molecules in the surface region may result in a (nearly) complete depletion of CSL molecules from the bulk region. This depletion is essentially complete for TRH at the two lowest temperatures considered.

The situation is inverted in the case of the HP wall. Here, it is water that presents an increased density (peaks around $z = l_z/2$ and $z = L_z - l_z/2$) in the immediate vicinity of the wall, while the CSLs present a decreased density (dips around $z = l_z/2$ and $z = L_z - l_z/2$). At intermediate distances, the situation is somewhat more complex. For the small CSLs, a layering effect can also be observed (small density peaks beyond the water peak). For the sugar CSLs, the CSL distributions are also heavily biased towards the wall surface, with broad peaks extending over a distance of 1–2 nm from the wall. The latter observation may rather result, however, from a kinetic effect (e.g. formation of a glassy matrix and 'dragging' of the sugar molecules along with the motion of the water molecules towards the wall surface) than from a thermodynamic one (these simulations are unlikely to have reached equilibrium; see above). Here also, the concentration of water molecules in the surface region may result in a partial depletion of water molecules from the bulk region (value of $p_{\mathrm{WAT}}(z)$ significantly below 1 in this region).

The values of the excess surface fraction $f_\alpha(d_c)$ (Equation (5)) for the species α (CSL, all carbon atoms; WAT, oxygen atom) in the simulations involving aqueous CSL solutions in the presence of the three types of wall and at the three temperatures considered are reported graphically in Figure 4. A positive value of $f_\alpha(d_c)$ for a given species (CSL or WAT) indicates a higher concentration of the corresponding species in the surface region relative to the bulk (with a limiting value of 1 for full affinity, i.e. the species is only found in the surface region). Conversely, a negative value indicates a lower concentration of the corresponding species in the surface region relative to the bulk (with a limiting value of -1 for

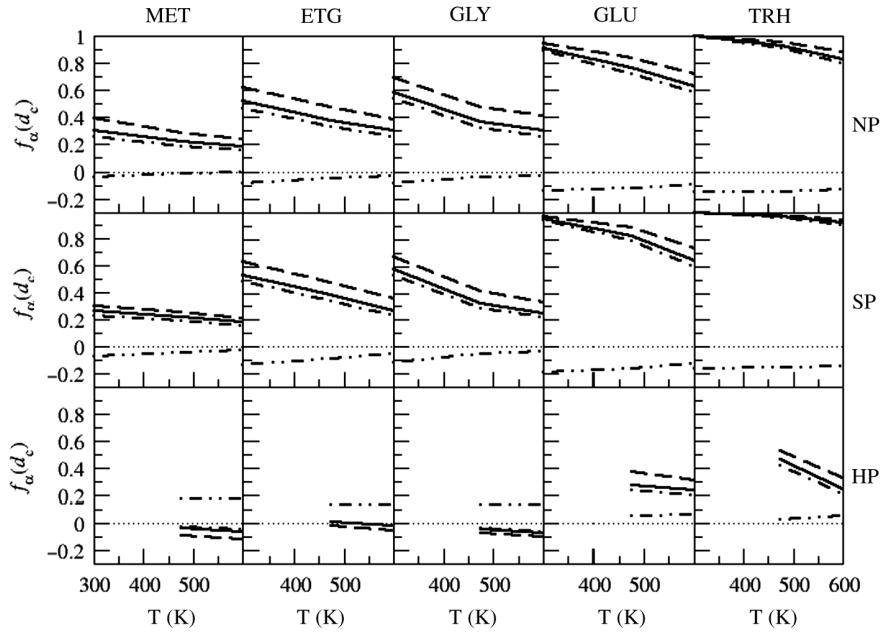

Figure 4. Excess surface fraction $f_\alpha(d_c)$ (Equation (5)) as a function of temperature T for the carbon atoms of the MET, ETG, GLY, GLU or TRH molecules and for the oxygen atom of the WAT molecules, corresponding to aqueous CSL solutions in the vicinity of a NP, SP or HP wall. The different lines correspond to different cut-off distances d_c from the wall surface: 0.85 nm (CSL only, dashed line); 1.30 nm (CSL, solid line; WAT, dot-dot-dashed line); or 1.60 nm (CSL only, dot-dashed line). A horizontal thin dotted line is drawn as well to mark the zero value.

full exclusion, i.e. the species is entirely absent from the surface region). Finally, a value of zero is expected for a species that is inert relative to the surface (i.e. bulk and surface concentrations of this species are identical). Note also that the parameter $f_\alpha(d_c)$ is constructed in such a way that it is independent of the wall thickness and solution volume (in the limit of large enough systems), and thus represents a property that only depends, for a given type of wall and at a given temperature, on the nature of the species (CSL or WAT) and the bulk concentration of the CSL solution (for a given choice of the cut-off parameter d_c). As evidenced by the results of Figure 4 for the CSL species, the qualitative results of this analysis are not affected by the selected value of d_c, and the quantitative differences also remain limited. For this reason, the discussion will be made with reference to a single cut-off value d_c of 1.30 nm (this value is sufficient to encompass the $p_\alpha(z)$ distribution peaks at the wall surface for all systems, except in the case of the TRH solutions at the HP wall), and $f_\alpha(d_c)$ will simply be written as f_α in this case.

In agreement with the previous discussion for $p_\alpha(z)$ (Figures 1–3), the systems involving NP and SP walls are characterised by positive values of f_{CSL} and negative values of f_{WAT} for all aqueous CSL solutions and at all temperatures. This shows again that all types of CSL evidence preferential affinity (compared to water) for these two types of walls. The two quantities systematically increase in magnitude upon increasing the size of the CSL molecule, and systematically decrease in magnitude upon increasing the temperature. The differences between the NP and SP walls are also relatively small, i.e. these two types of walls appear very similar with respect to the property monitored.

The situation is again different when considering the HP wall. Here, the aqueous solutions of the three smallest CSLs (MET, ETG and GLY) are characterised by negative values of f_{CSL} and positive values of f_{WAT}, the magnitude of which is small and nearly independent of the CSL type and temperature (475 vs. 600 K). Thus, these CSLs evidence preferential exclusion (compared to water) for this type of wall. In contrast, the sugar CSLs present positive values of both f_{CSL} and f_{WAT}. However, the latter observation may again result from an incomplete convergence of the simulations involving sugar CSLs in the presence of a HP wall (resulting from a very strong electrostatic interaction between the ionic surfaces and the aqueous solution).

The values of the excess surface fraction $f_\alpha(d_c)$ (Equation (5)) for the species α (CSL, all carbon atoms; WAT, oxygen atom) in the simulations involving pure liquid CSLs (MET, ETG and GLY only) or pure WAT in the presence of the three types of wall and at the three temperatures considered are reported graphically in Figure 5. Here also, the qualitative results of the analysis are not affected by the selected value of d_c (the quantitative differences also remain limited), so that only the cut-off value d_c of 1.30 nm will be considered and $f_\alpha(d_c)$ will simply be written as f_α in this case.

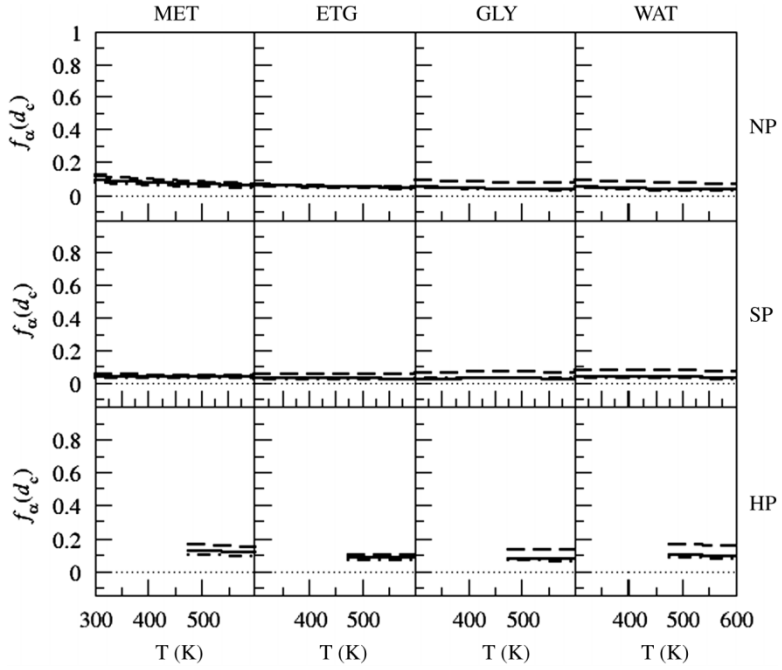

Figure 5. Excess surface fraction $f_\alpha(d_c)$ (Equation (5)) as a function of temperature T for the carbon atoms of the MET, ETG or GLY molecules and for the oxygen atom of the water (WAT) molecules, corresponding to pure CSL liquids or pure WAT in the vicinity of a NP, SP or HP wall. The different lines correspond to different cut-off distances d_c from the wall surface: 0.85 nm (dashed line); 1.30 nm (solid line); or 1.60 nm (dot-dashed line). A horizontal thin dotted line is drawn as well to mark the zero value.

In contrast to the observations made previously for the CSL aqueous solutions (Figure 4), f_α is close to zero for the four pure liquids and at all temperatures, indicating the absence of a significant driving force for the accumulation or the depletion of the surface region (compared to the bulk). For the NP and SP walls, the f_α values are of the order of 0.03–0.10, the largest values being observed for MET at the NP wall and at 300 K. In this case, a slight driving force towards the surface region probably results from attractive Lennard-Jones (dispersion) interactions with the densely packed LJPs of the wall, which may be slightly more favourable than the corresponding average dispersion interactions within the bulk liquid. The influence of these short-range interactions is not visible for the SP wall, where the liquid molecules and LJPs are kept apart by hydroxyl groups. It is also not visible for the other CSLs, where the larger size of the CSL molecule prevents a high density of CSL carbon atoms within the dispersion range of the wall, and for WAT, which has no carbon atom (the water oxygen has significantly smaller dispersion interactions). For the HP wall, the f_α values are somewhat more positive, of the order of 0.08–0.12. This slight preference of the liquid molecules for the surface region results from the strong electrostatic interaction with the ionic surfaces.

The comparison of the results for the CSL aqueous solutions (Figure 4) with those for the pure CSL liquids (Figure 5) clearly shows that the trends observed in the former case do not result from an intrinsic propensity of specific molecules to accumulate in or deplete from the surface region (relative to the bulk). Rather, they result from a differential propensity of CSL and WAT to do so (relative to the bulk CSL aqueous solution), i.e. from a preferential affinity (NP and SP walls) or exclusion (HP wall) of the CSL relative to WAT for the surface region.

The average numbers of H-bonds between the hydroxyl groups of a SP wall and its environment, for the simulations involving CSL aqueous solutions, pure liquid CSLs (MET, ETG and GLY only) or pure WAT at the three temperatures considered, are reported in Table 3. In addition to the expected overall reduction in the absolute numbers upon increasing the temperature, trends are similar at the three considered temperatures and the results will only be discussed considering the numbers at 300 K.

The average number of H-bonds is highest (123) in the simulation involving pure WAT. For the simulations of the pure liquid CSLs, the corresponding numbers are lower and increase in the sequence MET (34), ETG (85) and GLY (90). These trends are not related to any noticeable differences in the surface densities (relative to the bulk) for the considered systems (Figure 5). Instead, they are related to the effective molecular volumes associated with one oxygen atom in the different liquids (in the bulk as well as in the surface region). This effective volume can be estimated using the data in Table 2 (i.e. as $L_x L_y (L_z - l_z)(N_{CSL} \times n_O)^{-1}$, where $L_x = L_y = 3.36\,nm$) and increases in the sequence WAT ($0.031\,nm^3$) < GLY ($0.041\,nm^3$) < ETG ($0.049\,nm^3$) < MET ($0.070\,nm^3$). In other words, the number of H-bonds between the pure liquids and the SP wall correlates in a simple way with the number of oxygen atoms found in the surface region.

Table 3. Average numbers of H-bonds between the hydroxyl groups of the SP wall and its environment (at 300, 475 or 600 K), corresponding to CSL aqueous solutions, pure CSL liquids or WAT, and considering the CSLs MET, ETG, GLY, GLU (aqueous solution only) and TRH (aqueous solution only).

	Aqueous solution			Pure liquid
	CSL	WAT	All	All
$T = 300\,K$				
MET	13	87	100	34
ETG	49	58	107	85
GLY	42	71	113	90
GLU	50	61	110	–
TRH	41	61	103	–
WAT	–	–	–	123
$T = 475\,K$				
MET	12	72	84	39
ETG	25	66	91	65
GLY	20	77	97	71
GLU	36	57	93	–
TRH	45	52	97	–
WAT	–	–	–	109
$T = 600\,K$				
MET	11	66	77	34
ETG	18	65	83	54
GLY	15	73	89	59
GLU	27	57	84	–
TRH	34	53	87	–
WAT	–	–	–	99

Note: For the CSL aqueous solutions, the number of H-bonds specifically involving CSL and WAT molecules is also reported separately.

For the simulation of the CSL aqueous solutions, the total number of H-bonds, as contributed by both CSL and WAT molecules, remains about constant for all considered solutions (100–113 at 300 K), and only 10–20% lower than for pure WAT. The relative contribution of the CSL molecules to this total number is about 35–45%, except for MET (13%). Note that, at 475 and 600 K, this relative contribution increases (nearly) systematically with the size of the CSL molecule (the corresponding trend is not seen at 300 K). In summary, compared to the pure WAT situation, the CSLs in aqueous solution are seen to substitute WAT molecules at about one-third to one-half (only 13% for MET) of the H-bonding sites of the wall, with a limited decrease (10–20%) in the total number of H-bonds. These observations are qualitatively comparable with previous simulation results in the context of phospholipids membranes [6]. However, it should be kept in mind that the present model system (SP wall) is only an approximate representation for the surface

of a lipid membrane. In particular, the results may be sensitive to the selected spacing between the regularly spaced and isotropically oriented hydroxyl groups at the wall surface. The noticeably lower total number of H-bonds and extent of WAT replacement observed in the case of MET is probably related to the much higher effective volume associated with one oxygen atom in this molecule (see above) which limits the number of MET hydroxyl groups that can form H-bonds to the SP wall.

The thermodynamic parameters $\Delta A^{\circ}_{\alpha}$, $\Delta U^{\circ}_{\alpha}$ and $\Delta S^{\circ}_{\alpha}$ characterising the bulk-to-surface equilibrium (Equations (10)–(13)) for the species α (CSL, all carbon atoms; WAT, oxygen atom) in the simulations involving aqueous CSL solutions in the presence of the three types of wall and at the three temperatures considered are reported in Tables 4–6 (based on a cut-off distance d_c of 1.30 nm for defining the surface region). The corresponding parameters $\Delta_{exc}A^{\circ}_{CSL}$, $\Delta_{exc}U^{\circ}_{CSL}$ and $\Delta_{exc}S^{\circ}_{CSL}$ for the exchange reactions (Equations (14) and (15); i.e. the reaction substituting n_O water molecules by one CSL molecule in the surface region, n_O being the number of oxygen atoms in the CSL molecule) are also reported. In addition, the results for $\Delta A^{\circ}_{\alpha}$ are displayed graphically in Figure 6.

For the NP wall (Table 4 and Figure 6), the free energy ΔA°_{CSL} is negative and increases systematically in magnitude with increasing CSL size. It is moderately sensitive to temperature except for the sugar CSLs, where the value noticeably decreases in magnitude with increasing temperature. At 300 K, ΔA°_{CSL} evaluates to about -0.9, -1.8, -2.0, -5.4 and $-14.5\,kJ\,mol^{-1}$ for MET, ETG, GLY, GLU and TRH, respectively. This indicates the presence of a driving force for the CSL molecules towards the surface region under standard conditions (i.e. ideal solutions at identical concentrations in the bulk and surface regions). The corresponding energetic contribution ΔU°_{CSL}, which arises from the difference in interactions of the CSL molecules with the wall LJPs vs. with other molecules in the bulk and which is probably dominated by dispersion, is negative. The corresponding entropic contribution $-T\Delta S^{\circ}_{CSL}$, principally arising from the smaller volume accessible to the CSL molecules in the surface region (compared to the bulk) as well as from the more restricted molecular flexibility for larger CSLs, is typically positive except for MET and ETG ($-0.1\,kJ\,mol^{-1}$ at 300 K for both).

The free energy ΔA°_{WAT} for the NP wall is positive and increases systematically in magnitude with increasing CSL size. It is also moderately sensitive to temperature except for the sugar CSLs, where the value noticeably increases in magnitude with increasing temperature. At 300 K, ΔA°_{WAT} evaluates to about $1-3\,kJ\,mol^{-1}$ for the different CSL solutions. This indicates the presence of a driving force for the WAT molecules towards the bulk region under standard conditions. The corresponding energetic contribution ΔU°_{WAT}, arising from the difference in interactions of the WAT molecules with the wall LJPs vs. with other molecules in the bulk (probably dominated by H-bonding), is positive (about $1\,kJ\,mol^{-1}$ at 300 K). The corresponding entropic contribution $-T\Delta S^{\circ}_{CSL}$, principally arising from the smaller volume accessible to the WAT molecules in the surface region (compared to the bulk), is typically also positive except for GLY ($-0.1\,kJ\,mol^{-1}$ at 300 K).

It is now possible to compare the parameters for CSL and WAT for the NP wall in the form of the exchange parameters $\Delta_{exc}A^{\circ}_{CSL}$, $\Delta_{exc}U^{\circ}_{CSL}$ and $\Delta_{exc}S^{\circ}_{CSL}$. At 300 K, $\Delta_{exc}A^{\circ}_{CSL}$ is always negative and increases systematically in magnitude with the CSL size, evaluating to about -1.8, -4.8, -6.9, -21.2 and $-49.0\,kJ\,mol^{-1}$ for aqueous solutions of MET, ETG, GLY, GLU and TRH, respectively. The corresponding energetic contribution $\Delta_{exc}U^{\circ}_{CSL}$ is negative, and the corresponding entropic contribution $-T\Delta_{exc}S^{\circ}_{CSL}$ is typically also negative except for GLY ($0.6\,kJ\,mol^{-1}$ at 300 K).

In summary, the exchange reaction substituting n_O water molecules by a single CSL molecule in the surface region of a NP wall is favourable, both energetically and (except for GLY) entropically, for all polyhydroxylated CSLs considered. The associated driving force also systematically increases in magnitude with increasing CSL size, and is particularly large for the sugar CSLs.

For the SP wall (Table 5 and Figure 6), the results are qualitatively very similar to those for the NP wall. The free energy ΔA°_{CSL} is also negative, increases in magnitude with increasing CSL size and significantly decreases in magnitude with increasing temperature for the sugar CSLs only. At 300 K, the ΔA°_{CSL} values are very close to the corresponding values for the NP wall, except for the sugar CSLs, where they are more negative by about $1.5-3.5\,kJ\,mol^{-1}$. The corresponding energetic contribution ΔU°_{CSL} is also negative. At 300 K, the ΔU°_{CSL} values are very close to the corresponding values for the NP wall, except for the sugar CSLs, where they are more negative by about $3-5\,kJ\,mol^{-1}$. The corresponding entropic contribution $-T\Delta S^{\circ}_{CSL}$ is typically also positive except for MET and ETG. At 300 K, the $-T\Delta S^{\circ}_{CSL}$ values are very close to the corresponding values for the NP wall, except for the sugar CSLs, where they are less negative by about $1.5\,kJ\,mol^{-1}$.

The free energy ΔA°_{WAT} for the SP wall is also positive, increases in magnitude with increasing CSL size and significantly increases in magnitude with increasing temperature for the sugar CSLs only. At 300 K, the ΔA°_{WAT} values are all very close to the corresponding values for the NP wall. The corresponding energetic and entropic contributions ΔU°_{WAT} and $-T\Delta S^{\circ}_{CSL}$ are also of comparable magnitudes.

The exchange free energy $\Delta_{exc}A^{\circ}_{CSL}$ for the SP wall is also always negative and increases systematically in

Table 4. Standard thermodynamic parameters (Helmholtz free energy, energy, entropy) $\Delta A^{\circ}_{\alpha}$, $\Delta U^{\circ}_{\alpha}$ and $\Delta S^{\circ}_{\alpha}$ of the bulk-to-surface equilibrium for species α, and thermodynamic parameters $\Delta_{exc}A^{\circ}_{CSL}$, $\Delta_{exc}U^{\circ}_{CSL}$ and $\Delta_{exc}S^{\circ}_{CSL}$ of exchange calculated according to Equations (10)–(15) (using $d_c = 1.30$ nm) for the CSL aqueous solutions at a NP wall.

NP wall		CSL			WAT			Equation (15)		
Mixture	T (K)	$\Delta A^{\circ}_{\alpha}$ (kJ mol^{-1})	$\Delta U^{\circ}_{\alpha}$ (kJ mol^{-1})	$-T\Delta S^{\circ}_{\alpha}$ (kJ mol^{-1})	$\Delta A^{\circ}_{\alpha}$ (kJ mol^{-1})	$\Delta U^{\circ}_{\alpha}$ (kJ mol^{-1})	$-T\Delta S^{\circ}_{\alpha}$ (kJ mol^{-1})	$\Delta_{exc}A^{\circ}_{CSL}$ (kJ mol^{-1})	$\Delta_{exc}U^{\circ}_{CSL}$ (kJ mol^{-1})	$-T\Delta_{exc}S^{\circ}_{CSL}$ (kJ mol^{-1})
MET	300	−0.9	−0.8	−0.1	0.9	0.8	0.1	−1.8	−1.6	−0.1
	475	−0.9	−1.0	0.0	0.9	1.0	0.0	−1.9	−1.9	0.1
	600	−0.9	−1.2	0.3	0.9	1.2	−0.3	−1.7	−2.3	0.6
ETG	300	−1.8	−1.7	−0.1	1.5	1.3	0.2	−4.8	−4.3	−0.6
	475	−1.8	−1.9	0.1	1.7	1.5	0.1	−5.1	−4.9	−0.2
	600	−1.7	−2.2	0.5	1.6	1.9	−0.2	−4.9	−5.9	1.0
GLY	300	−2.0	−2.4	0.4	1.6	1.7	−0.1	−6.9	−7.5	0.6
	475	−1.7	−2.1	0.4	1.6	1.6	0.0	−6.5	−6.9	0.4
	600	−1.7	−1.7	0.0	1.6	1.5	0.2	−6.6	−6.1	−0.5
GLU	300	−5.4	−5.6	0.2	2.6	1.2	1.5	−21.2	−12.6	−8.5
	475	−5.2	−6.3	1.0	3.5	0.9	2.5	−26.2	−11.9	−14.2
	600	−4.7	−7.2	2.5	4.2	0.6	3.6	−30.2	−10.9	−19.3
TRH	300	−14.5	−22.8	8.2	2.9	0.5	2.3	−49.0	−29.1	−19.9
	475	−9.8	−19.4	9.6	4.2	1.2	3.1	−60.6	−33.6	−27.0
	600	−8.5	−14.6	6.1	4.8	2.1	2.7	−66.1	−39.9	−26.2

Notes: Values for $T\Delta S^{\circ}_{\alpha}$ at $T = 300$, 475 and 600 K were calculated using Equation (12), from the differences in free energies $[\Delta A^{\circ}_{\alpha}(T = 475\,\text{K}) - \Delta A^{\circ}_{\alpha}(T = 300\,\text{K})]$, $[\Delta A^{\circ}_{\alpha}(T = 600\,\text{K}) - \Delta A^{\circ}_{\alpha}(T = 300\,\text{K})]$ and $[\Delta A^{\circ}_{\alpha}(T = 600\,\text{K}) - \Delta A^{\circ}_{\alpha}(T = 475\,\text{K})]$, respectively.

Table 5. Standard thermodynamic parameters (Helmholtz free energy, energy, entropy) $\Delta A^{\circ}_{\alpha}$, $\Delta U^{\circ}_{\alpha}$ and $\Delta S^{\circ}_{\alpha}$ of the bulk-to-surface equilibrium for species α, and thermodynamic parameters $\Delta_{exc}A^{\circ}_{CSL}$, $\Delta_{exc}U^{\circ}_{CSL}$ and $\Delta_{exc}S^{\circ}_{CSL}$ of exchange calculated according to Equations (10)–(15) (using $d_c = 1.30$ nm) for the CSL aqueous solutions at a SP wall.

SP wall		CSL			WAT			Equation (15)		
Mixture	T (K)	$\Delta A^{\circ}_{\alpha}$ (kJ mol^{-1})	$\Delta U^{\circ}_{\alpha}$ (kJ mol^{-1})	$-T\Delta S^{\circ}_{\alpha}$ (kJ mol^{-1})	$\Delta A^{\circ}_{\alpha}$ (kJ mol^{-1})	$\Delta U^{\circ}_{\alpha}$ (kJ mol^{-1})	$-T\Delta S^{\circ}_{\alpha}$ (kJ mol^{-1})	$\Delta_{exc}A^{\circ}_{CSL}$ (kJ mol^{-1})	$\Delta_{exc}U^{\circ}_{CSL}$ (kJ mol^{-1})	$-T\Delta_{exc}S^{\circ}_{CSL}$ (kJ mol^{-1})
MET	300	−0.7	−0.4	−0.4	0.7	0.3	0.4	−1.5	−0.7	−0.8
	475	−1.0	−0.6	−0.4	1.0	0.6	0.4	−1.9	−1.2	−0.7
	600	−1.0	−0.9	0.0	1.0	0.9	0.0	−1.9	−1.9	0.0
ETG	300	−1.8	−1.8	−0.1	1.6	1.4	0.2	−5.0	−4.5	−0.6
	475	−1.9	−2.3	0.4	1.7	1.9	−0.2	−5.4	−6.1	0.7
	600	−1.5	−3.0	1.5	1.5	2.7	−1.2	−4.6	−8.4	3.8
GLY	300	−2.0	−2.8	0.8	1.7	2.0	−0.4	−6.9	−8.9	2.0
	475	−1.5	−2.4	0.9	1.4	1.9	−0.5	−5.8	−8.0	2.3
	600	−1.4	−1.9	0.4	1.4	1.7	−0.3	−5.5	−6.8	1.3
GLU	300	−7.1	−8.7	1.6	2.9	1.3	1.6	−24.4	−16.2	−8.2
	475	−6.2	−9.7	3.5	3.8	2.4	1.4	−29.1	−24.2	−5.0
	600	−4.9	−11.0	6.1	3.8	4.0	−0.3	−27.5	−35.3	7.8
TRH	300	−18.2	−28.1	9.9	2.9	0.3	2.7	−53.5	−31.5	−22.0
	475	−12.5	−23.4	10.9	4.5	0.7	3.8	−66.3	−31.9	−34.4
	600	−11.3	−16.9	5.5	5.3	1.3	4.0	−75.2	−32.5	−42.8

Notes: Values for $T\Delta S^{\circ}_{\alpha}$ at $T = 300$, 475 and 600 K were calculated using Equation (12), from the differences in free energies $[\Delta A^{\circ}_{\alpha}(T = 475\,\text{K}) - \Delta A^{\circ}_{\alpha}(T = 300\,\text{K})]$, $[\Delta A^{\circ}_{\alpha}(T = 600\,\text{K}) - \Delta A^{\circ}_{\alpha}(T = 300\,\text{K})]$ and $[\Delta A^{\circ}_{\alpha}(T = 600\,\text{K}) - \Delta A^{\circ}_{\alpha}(T = 475\,\text{K})]$, respectively.

Table 6. Standard thermodynamic parameters (Helmholtz free energy, energy, entropy) $\Delta A^{\circ}_{\alpha}$, $\Delta U^{\circ}_{\alpha}$ and $\Delta S^{\circ}_{\alpha}$ of the bulk-to-surface equilibrium for species α, and thermodynamic parameters $\Delta_{exc}A^{\circ}_{CSL}$, $\Delta_{exc}U^{\circ}_{CSL}$ and $\Delta_{exc}S^{\circ}_{CSL}$ of exchange calculated according to Equations (10)–(15) (using $d_c = 1.30$ nm) for the CSL aqueous solutions at a HP wall.

HP wall		CSL			WAT			Equation (15)		
Mixture	T (K)	$\Delta A^{\circ}_{\alpha}$ (kJ mol^{-1})	$\Delta U^{\circ}_{\alpha}$ (kJ mol^{-1})	$-T\Delta S^{\circ}_{\alpha}$ (kJ mol^{-1})	$\Delta A^{\circ}_{\alpha}$ (kJ mol^{-1})	$\Delta U^{\circ}_{\alpha}$ (kJ mol^{-1})	$-T\Delta S^{\circ}_{\alpha}$ (kJ mol^{-1})	$\Delta_{exc}A^{\circ}_{CSL}$ (kJ mol^{-1})	$\Delta_{exc}U^{\circ}_{CSL}$ (kJ mol^{-1})	$-T\Delta_{exc}S^{\circ}_{CSL}$ (kJ mol^{-1})
MET	300									
	475	0.9	−0.3	1.2	−0.9	0.3	−1.2	1.8	−0.6	2.4
	600	1.2	−0.3	1.5	−1.2	0.3	−1.5	2.4	−0.6	3.0
ETG	300									
	475	0.5	−0.5	1.0	−0.5	0.5	−1.0	1.6	−1.4	3.0
	600	0.8	−0.5	1.3	−0.8	0.5	−1.3	2.4	−1.4	3.8
GLY	300									
	475	0.7	−0.4	1.2	−0.7	0.4	−1.2	3.0	−1.8	4.8
	600	1.1	−0.4	1.5	−1.1	0.4	−1.5	4.2	−1.8	6.0
GLU	300									
	475	−0.9	−1.0	0.2	0.8	0.9	−0.1	−5.7	−6.7	1.0
	600	−0.8	−1.0	0.2	0.8	0.9	−0.2	−5.5	−6.7	1.2
TRH	300									
	475	−1.7	−4.7	3.0	1.5	3.9	−2.4	−19.5	−51.4	32.0
	600	−0.9	−4.7	3.8	0.8	3.9	−3.0	−11.1	−51.4	40.4

Notes: Values for $T\Delta S^{\circ}_{\alpha}$ at $T = 475$ and 600 K were calculated using Equation (12), from the difference in free energy $[\Delta A^{\circ}_{\alpha}(T = 600\,\text{K}) - \Delta A^{\circ}_{\alpha}(T = 475\,\text{K})]$.

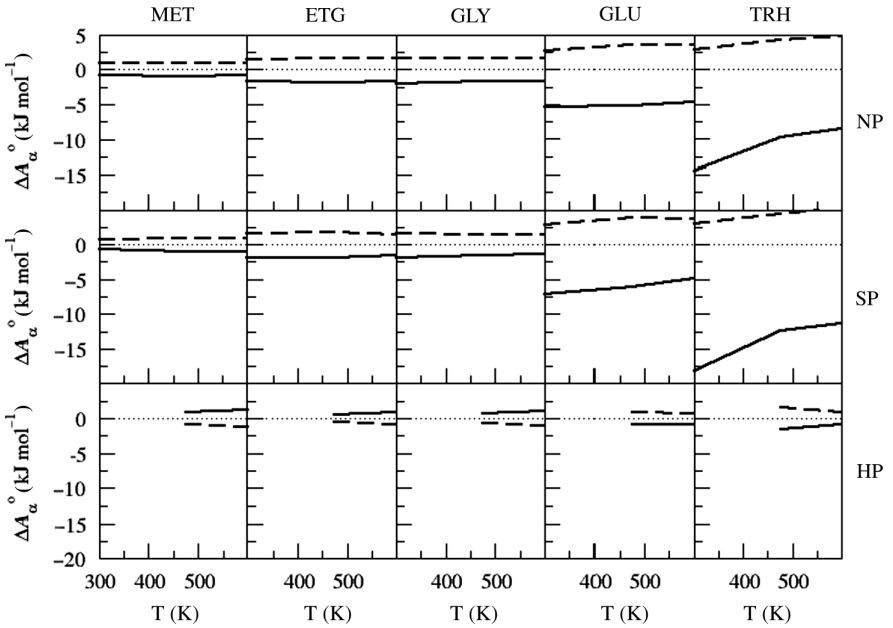

Figure 6. Standard (Helmholtz) free energy ΔA_α° (Equations (10) and (11), using $d_c = 1.30$ nm) of the bulk-to-surface equilibrium as a function of the temperature T for the carbon atoms of the MET, ETG, GLY, GLU or TRH molecules (solid lines) and for the oxygen atom of the water (WAT) molecules (dashed lines), corresponding to aqueous CSL solutions in the vicinity of a NP, SP or HP wall. A horizontal thin dotted line is drawn as well to mark the zero value.

magnitude with the CSL size. At 300 K, the $\Delta_{exc}A^\circ_{CSL}$ values are all very close to the corresponding values for the NP wall, except for the sugar CSLs, where they are more negative by about 1.5–3 kJ mol^{-1}. The corresponding energetic and entropic contributions $\Delta_{exc}U^\circ_{CSL}$ and $-T\Delta_{exc}S^\circ_{CSL}$ are also of comparable magnitudes, except for the sugar CSLs, where $\Delta_{exc}U^\circ_{CSL}$ is more negative by about 2–3.5 kJ mol^{-1}.

In summary, the exchange reaction substituting n_O water molecules by a single CSL molecule in the surface region of a SP wall is favourable, both energetically and entropically, for all polyhydroxylated CSLs considered, as it was the case for the NP wall. The associated driving force systematically increases in magnitude with increasing CSL size, and appears to be very similar to that for the NP wall, except for the sugar CSLs, where the driving force is somewhat stronger (this change can be traced to a slightly more negative ΔA°_{CSL} value). This driving force is again particularly large for the sugar CSLs.

For the HP wall (Table 6 and Figure 6), the situation is qualitatively different compared to the NP and SP walls. Because the simulations at 300 K appear unconverged for the sugar CSLs (Figure 1), the results at 475 K will be discussed. In contrast to the NP and SP walls, the free energy ΔA°_{CSL} is now positive for the small CSLs MET, ETG and GLY (about 1 kJ mol^{-1}). It remains negative for the sugar CSLs, namely -0.9 and -1.7 for GLU and TRH, respectively, but with a magnitude lower by about 5–10 kJ mol^{-1} (compared to the NP or SP walls at 475 K). For the small CSLs, this indicates the presence of a driving force for the CSL molecules away from the surface region, while for the sugar CSLs, the driving force towards the surface region is largely reduced compared to the NP and SP walls. The corresponding energetic contribution ΔU°_{CSL} is still negative and the corresponding entropic contribution $-T\Delta S^\circ_{CSL}$ is still positive. However, both terms are much smaller in magnitude compared to the NP and SP walls, the former being more significantly reduced especially for the sugar CSLs, which causes the observed trends in ΔA°_{CSL}.

In contrast to the NP and SP walls, the free energy ΔA°_{WAT} for the HP wall is now negative for the solutions of the small CSLs MET, ETG and GLY (about -1 kJ mol^{-1}). It remains positive for the solutions of the sugar CSLs, namely 0.8 and 1.5 for GLU and TRH, respectively, but with a magnitude lower by about 3 kJ mol^{-1} (compared to the NP or SP walls at 475 K). For the solutions of the small CSLs, this indicates the presence of a driving force for the WAT molecules towards the surface region under standard conditions, while for the sugar CSLs, the driving force towards the bulk region is significantly reduced compared to the NP and SP walls. The corresponding energetic contribution ΔU°_{WAT} is still positive but the corresponding entropic contribution $-T\Delta S^\circ_{WAT}$ is now negative for the solutions of all CSLs, which causes the observed trends in ΔA°_{WAT}.

In contrast to the NP and SP walls, the exchange free energy $\Delta_{exc}A^\circ_{CSL}$ for the HP wall is now positive for the small CSLs, namely 1.8, 1.6 and 3.0 kJ mol^{-1} for MET, ETG and GLY, respectively. It remains negative for the

sugar CSLs, namely −5.7 and −19.5 for GLU and TRH, respectively, but with a magnitude lower by about 20–45 kJ mol^{-1} (compared to the NP or SP walls at 475 K). The corresponding energetic contribution $\Delta_{exc}U^{\circ}_{CSL}$ is still negative but the corresponding entropic contribution $-T\Delta_{exc}S^{\circ}_{CSL}$ is now positive for all CSLs, which causes the observed trends in $\Delta_{exc}A^{\circ}_{CSL}$.

In summary, the exchange reaction substituting n_O water molecules by a single CSL molecule in the surface region of a HP wall is favourable energetically but unfavourable entropically for all polyhydroxylated CSLs considered. The balance becomes increasingly favourable with increasing CSL size. As a result, the small CSLs show preferential exclusion while the sugar CSLs still show preferential affinity, but with a strongly reduced driving force compared to the NP and SP walls.

Finally, normalised probability distribution functions $p_\alpha(z)$ evaluated separately for sites α corresponding to the carbon or oxygen atoms of the CSLs in the simulations involving aqueous CSL solutions in the presence of the three types of wall (NP, SP and HP) are displayed in Figure 7 for the simulations at 300 K (NP, SP) or 475 K (HP). The corresponding profiles evaluated at the other temperatures present similar qualitative trends (data not shown). Note that the curves are only displayed in the range $[0; \frac{1}{2}L_z]$.

The relative peak positions in these two types of profiles provide information on the orientational preferences of the CSL molecules close to the wall. The $p_\alpha(z)$ profiles at the SP and HP walls exhibit a first CSL oxygen peak at a smaller distance compared to the first carbon peak. This indicates that the CSL molecules preferentially orient their hydroxyl groups towards the (semi-)polar wall surface, probably as a result of energetically favourable electrostatic (H-bonding) interactions. In contrast, the corresponding $p_\alpha(z)$ profiles for MET, ETG and GLY at the NP wall suggest that these CSL molecules preferentially orient their alkyl groups towards the NP wall surface. Interestingly, however, the $p_\alpha(z)$ profiles for the sugar oxygen and carbon atoms of GLU and TRH at the NP wall do not hint at a similar preference, probably due to the geometrical restrictions imposed by the molecular framework of the sugars. The first peaks in the $p_\alpha(z)$ profiles even suggest that the sugar oxygen atoms can be found closer to the NP surface than the carbon atoms (especially for TRH). Whether this qualitative difference between the orientational preferences of sugars and smaller CSLs at NP walls is meaningful (e.g. has implications in the context of membrane bioprotection) will be investigated in future work.

4. Conclusions

The interaction of polyhydroxylated CSLs with lipid bilayers has been previously suggested (based on simulation results along with available experimental data) to result from the interplay between an alcohol-like mechanism and a sugar-like mechanism [6]. In the present study, the sugar-like mechanism was investigated more specifically in the context of an interface modelled as a rigid wall of LJPs. Three types of walls were considered, namely walls with either NP (unaltered LJPs), SP (partial

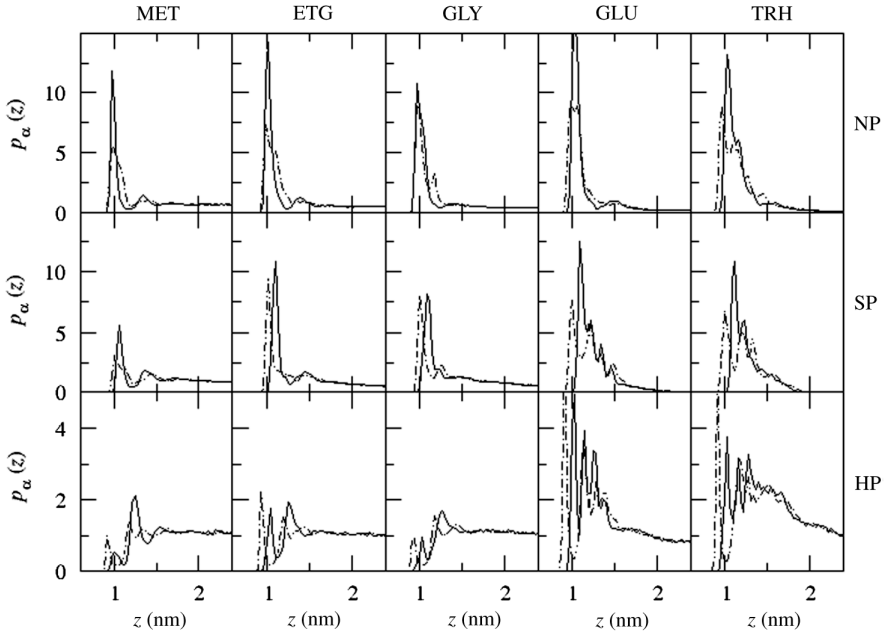

Figure 7. Normalised probability distribution functions $p_\alpha(z)$ (Equation (1)) for the carbon atoms (solid lines) and the oxygen atoms (dot-dashed lines) of the MET, ETG, GLY, GLU or TRH molecules, corresponding to aqueous CSL solutions in the vicinity of a NP or a SP wall at $T = 300$ K, and in the vicinity of a HP wall at $T = 475$ K. Note that the curves are only displayed in the range $[0; \frac{1}{2}L_z]$.

hydroxylation of the surface LJPs) or HP (partial ionisation of the surface LJPs) surfaces. These walls were exposed either to aqueous solutions of the different polyhydroxylated CSLs (MET, ETG, GLY, GLU or TRH), to the different pure liquid CSLs (MET, ETG and GLY only) or to pure water (WAT). The explicit-solvent MD simulations of these systems, at constant volume and at three different temperatures (300, 475 or 600 K), were analysed in terms of preferential affinity or exclusion of the CSL for the wall surface (compared to WAT), H-bonding, preferential CSL orientation towards the wall surface, and derived thermodynamic parameters (bulk-to-surface equilibrium, exchange equilibrium). The main results can be summarised as follows.

All polyhydroxylated CSLs considered show preferential affinity (compared to WAT) for the NP and SP walls. This effect, which increases systematically in magnitude with increasing CSL size, is related to the favourable driving force of the exchange reaction substituting n_O water molecules by a single CSL molecule in the surface region, where n_O is the number of oxygen atoms per CSL molecule. This process is favoured both energetically (more favourable interactions of the CSL molecules with the surface as opposed to within the bulk; more favourable interactions of the n_O water molecules within the bulk as opposed to with the surface) and entropically (one CSL molecule with restricted translational freedom vs. n_O water molecules with increased translational freedom). The free energy associated with this exchange is particularly large for the sugar CSLs (about -20 and $-50\,\mathrm{kJ\,mol^{-1}}$ for GLU and TRH, respectively). The results for the NP and SP walls are very similar, except for a somewhat increased driving force (about $1.5-3\,\mathrm{kJ\,mol^{-1}}$) for the sugar CSLs in the latter case. In the case of the SP wall, the substitution of WAT by CSL molecules in the surface region is only accompanied by a moderate decrease (10–20%, largely independent of the nature of the CSL) in the number of H-bonds between the surface and its solution environment (comparing pure WAT with aqueous CSL solutions).

These features are compatible with the sugar-like mechanism [6], with the proviso that this mechanism overlooked the favourable energetic contribution to the exchange reaction (predominantly related to the transfer of water molecules from the surface region to the bulk) and attributed the associated driving force to entropy only. It is also in line with the observation of preferential affinity of sugars towards phospholipid membranes reported by nearly all simulation studies to date [6,45,48–54], as well as by many experimental studies [3,4,19,20,30,32–34], although other experimental studies [24,40,41] support preferential exclusion instead.

The results for the HP wall are qualitatively different from those for the NP and SP walls. The small polyhydroxylated CSLs considered (MET, ETG and GLY) show preferential exclusion (compared to WAT) for the HP wall. The sugar CSLs still show preferential affinity, but with a much more limited driving force for the exchange reaction. Intuitively, these changes may be understood by the observation that the effective dielectric permittivity of the surface region (i.e. its ability to solvate surface charges) plays an increasingly important role upon increasing the polarity of the wall. In turn, this effective permittivity is likely to increase with the water content: bulk liquid permittivities of WAT, MET, ETG and GLY at 298 K are 78.5 [106], 32.6 [107], 37.7 [108] and 45 [109], respectively (GLY value at 291 K). In other words, a HP wall will preferentially attract WAT molecules over CSL ones, because WAT is most effective in terms of electrostatic solvation.

The observation of a trend towards the reduction in the preferential affinity (or even a shift towards preferential exclusion) of polyhydroxylated CSLs for model surfaces upon increasing the polarity of the surface is particularly interesting in the context of the bioprotection phenomenon. As pointed out in the introduction of this article, based on recent studies concerning the dielectric properties of the surfaces of membranes [56] and of water-soluble proteins [55], and considering the typically high density of charged amino acid side chains at the aqueous interface of the latter, it is reasonable to regard protein surfaces as being more polar than membrane surfaces. Accepting the existence of such a difference between the two types of biomolecules in terms of surface polarity, the observed reduction in the preferential affinity of CSLs for the Lennard-Jones walls upon increasing their surface polarity could explain why combined experimental and theoretical evidence tends to support a preferential affinity of sugar molecules for membrane surfaces [6,45,48–54] (see, however, [24,40,41]) and a preferential exclusion of sugar molecules for protein surfaces [22,23,25,37–39, 42–47] (see, however, [14,17,18,21,35,36]).

Clearly, this work only represents a first step towards the detailed characterisation of interfacial effects relevant for the interaction of polyhydroxylated CSLs with biomolecular surfaces (as involved in bioprotection phenomena). Keeping the simplicity and convergence advantages afforded by the use of model walls, further work will involve more systematic analyses of the effect of the CSL concentration as well as of the wall polarity, curvature (i.e. considering walls with non-planar surfaces) and functionalisation (e.g. more realistic representation of a typical membrane or protein surface).

Acknowledgements

Financial support from the National Centre in Competence in Research (NCCR) in Structural Biology and from Grant No. 200021-109227 of the Swiss National Science Foundation is gratefully acknowledged.

Note

1. Present address: Leiden/Amsterdam Center for Drug Research, Division of Molecular and Computational Toxicology, Vrije Universiteit Amsterdam, De Boelelaan 1083, 1081 HV Amsterdam, The Netherlands.

References

[1] G.R.A. Hunt and I.C. Jones, *A H-1-NMR investigation of the effects of ethanol and general-anesthetics on ion channels and membrane-fusion using unilamellar phospholipid-membranes*, Biochim. Biophys. Acta 736 (1983), pp. 1–10.

[2] W.R. Klemm, *Biological water and its role in the effects of alcohol*, Alcohol 15 (1998), pp. 249–267.

[3] L.M. Crowe, *Lessons from nature: The role of sugars in anhydrobiosis*, Comp. Biochem. Physiol. A 131 (2002), pp. 505–513.

[4] J.H. Crowe, L.M. Crowe, W.F. Wolkers, A.E. Oliver, X.C. Ma, J.H. Auh, M.K. Tang, S.J. Zhu, J. Norris, and F. Tablin, *Stabilization of dry mammalian cells: Lessons from nature*, Integr. Comp. Biol. 45 (2005), pp. 810–820.

[5] A. Tunnacliffe and J. Lapinski, *Resurrecting Van Leeuwenhoek's rotifers: A reappraisal of the role of disaccharides in anhydrobiosis*, Philos. Trans. R. Soc. B 358 (2003), pp. 1755–1771.

[6] C.S. Pereira and P.H. Hünenberger, *The influence of polyhydroxylated compounds on a hydrated phospholipid bilayer: A molecular dynamics study*, Mol. Sim. 34 (2008), pp. 403–420.

[7] N. Franks and W.R. Lieb, *Partitioning of long-chain alcohols into lipid bilayers – Implications for mechanisms of general-anesthesia*, Proc. Natl Acad. Sci. USA 83 (1986), pp. 5116–5120.

[8] J.T. Mohr, G.W. Gribble, S.S. Lin, R.G. Eckenhoff, and R.S. Cantor, *Anesthetic potency of two novel synthetic polyhydric alkanols longer than the n-alkanol cutoff: Evidence for a bilayer-mediated mechanism of anesthesia?* J. Med. Chem. 48 (2005), pp. 4172–4176.

[9] R.S. Cantor, *The lateral pressure profile in membranes: A physical mechanism of general anesthesia*, Biochemistry 36 (1997), pp. 2339–2344.

[10] Z. Hubalek, *Protectants used in the cryopreservation of microorganisms*, Cryobiology 46 (2003), pp. 205–229.

[11] B.J. Fuller, *Cryoprotectants: The essential antifreezes to protect life in the frozen state*, Cryoletters 25 (2004), pp. 375–388.

[12] J.H. Crowe, L.M. Crowe, and D. Chapman, *Preservation of membranes in anhydrobiotic organisms – The role of trehalose*, Science 223 (1984), pp. 701–703.

[13] J.H. Crowe, F.A. Hoekstra, and L.M. Crowe, *Anhydrobiosis*, Annu. Rev. Physiol. 54 (1992), pp. 579–599.

[14] J.F. Carpenter, S.J. Prestrelski, T.J. Anchordoguy, and T. Arakawa, *Interactions of stabilizers with proteins during freezing and drying*, in *Formulation and Delivery of Proteins and Peptides*, J.L. Cleland, and R. Langer, eds., American Chemical Society, Washington, DC, 1994, pp. 134–147.

[15] J.H. Crowe, L.M. Crowe, J.F. Carpenter, S. Prestrelski, F.A. Hoekstra, P. de Araujo, and A.D. Panek, *Anhydrobiosis: Cellular adaptation to extreme dehydration*, in *Handbook of Physiology*, W.H. Dantzler, ed., Oxford University Press, Oxford, UK, 1997, pp. 1445–1477.

[16] J.H. Crowe, J.S. Clegg, and L.M. Crowe, *Anhydrobiosis: The water replacement hypothesis*, in *The Properties of Water in Foods (ISO-POW 6)*, D.S. Reid, ed., Chapman and Hall, New York, 1998, pp. 440–455.

[17] M. Sola-Penna and J.R. Meyer-Fernandes, *Stabilization against thermal inactivation promoted by sugars on enzyme structure and function: Why is trehalose more effective than other sugars?* Arch. Biochem. Biophys. 360 (1998), pp. 10–14.

[18] S.D. Allison, B. Chang, T.W. Randolph, and J.F. Carpenter, *Hydrogen bonding between sugar and protein is responsible for inhibition of dehydration-induced protein unfolding*, Arch. Biochem. Biophys. 365 (1999), pp. 289–298.

[19] C. Lambruschini, A. Relini, A. Ridi, L. Cordone, and A. Gliozzi, *Trehalose interacts with phospholipid polar heads in Langmuir monolayers*, Langmuir 16 (2000), pp. 5467–5470.

[20] M.D. Luzardo, F. Amalfa, A.M. Nuñez, S. Díaz, A.C. Biondi de Lopez, and E.A. Disalvo, *Effect of trehalose and sucrose on the hydration and dipole potential of lipid bilayers*, Biophys. J. 78 (2000), pp. 2452–2458.

[21] P. Zancan and M. Sola-Penna, *Trehalose and glycerol stabilize and renature yeast inorganic pyrophosphatase inactivated by very high temperatures*, Arch. Biochem. Biophys. 444 (2005), pp. 52–60.

[22] S.N. Timasheff, *The control of protein stability and association by weak-interactions with water*, in *Biophysics of Water*, F. Franks and S. Mathias, eds., Wiley, New York, 1982, pp. 70–72.

[23] G.F. Xie and S.N. Timasheff, *The thermodynamic mechanism of protein stabilization by trehalose*, Biophys. Chem. 64 (1997), pp. 25–43.

[24] P. Westh, *Glucose, sucrose and trehalose are partially excluded from the interface of hydrated DMPC bilayers*, Phys. Chem. Chem. Phys. 10 (2008), pp. 4110–4112.

[25] S. Belton and A.M. Gil, *IR and Raman-spectroscopic studies of the interaction of trehalose with hen egg-white lysozyme*, Biopolymers 34 (1994), pp. 957–961.

[26] R.J. Williams and A.C. Leopold, *The glassy state in corn embryos*, Plant Physiol. 89 (1989), pp. 977–981.

[27] W.Q. Sun, T.C. Irving, and A.C. Leopold, *The role of sugar, vitrification and membrane phase-transition in seed desiccation tolerance*, Physiol. Plantarum 90 (1994), pp. 621–628.

[28] W.Q. Sun and A.C. Leopold, *Glassy state and seed storage ability – A viability equation analysis*, Ann. Bot. 74 (1994), pp. 601–604.

[29] W.Q. Sun, A.C. Leopold, L.M. Crowe, and J.H. Crowe, *Stability of dry liposomes in sugar glasses*, Biophys. J. 70 (1996), pp. 1769–1776.

[30] W.Q. Sun and A.C. Leopold, *Cytoplasmic vitrification acid survival of anhydrobiotic organisms*, Comp. Biochem. Physiol. A 117 (1997), pp. 327–333.

[31] I. Köper, S. Combet, W. Petry, and M.-C. Bellissent-Funel, *Dynamics of C-phycocyanin in various deuterated trehalose/-water environments measured by quasielastic and elastic neutron scattering*, Eur. Biophys. J. 37 (2008), pp. 739–748.

[32] J.H. Crowe, J.F. Carpenter, and L.M. Crowe, *The role of vitrification in anhydrobiosis*, Annu. Rev. Physiol. 60 (1998), pp. 73–103.

[33] J.S. Clegg, *Cryptobiosis – A peculiar state of biological organization*, Comp. Biochem. Physiol. B 128 (2001), pp. 613–624.

[34] J.H. Crowe, A.E. Oliver, and F. Tablin, *Is there a single biochemical adaptation to anhydrobiosis?* Integr. Comp. Biol. 42 (2002), pp. 497–503.

[35] D.E. Khoshtariya, T.D. Dolidze, S. Seifert, D. Sarauli, G. Lee, and R. van Eldik, *Kinetic, thermodynamic, and mechanistic patterns for free (unbound) cytochrome c at Au/SAM junctions: Impact of electronic coupling, hydrostatic pressure, and stabilizing/denaturing additives*, Chem. Eur. J. 12 (2006), pp. 7041–7056.

[36] K. Sasanuma, Y. Seshimo, E. Hashimoto, Y. Ike, and S. Kojima, *Trehalose bioprotective effects in lysozyme aqueous solution studies by Brillouin scattering and calorimetric measurements*, Jpn J. Appl. Phys. 47 (2008), pp. 3843–3846.

[37] S.N. Timasheff, *Control of protein stability and reactions by weakly interacting cosolvents: The simplicity of the complicated*, Adv. Protein Chem. 51 (1998), pp. 355–432.

[38] A.M. Massari, I.J. Finkelstein, B.L. McCain, A. Goj, X. Wen, K.L. Bren, R.F. Loring, and M.D. Fayer, *The influence of aqueous vs. glassy solvents on protein dynamics: Vibrational echo experiments and molecular dynamics simulations*, J. Am. Chem. Soc. 127 (2005), pp. 14279–14289.

[39] B. Varga, F. Migliardo, E. Takacs, B. Vertessy, S. Magazù, and C. Mondelli, *Neutron scattering studies on dUTPase complex in the presence of bioprotectant systems*, Chem. Phys. 345 (2008), pp. 250–258.

[40] B. Demé, M. Dubois, and T. Zemb, *Swelling of a lecithin lamellar phase induced by small carbohydrate solutes*, Biophys. J. 82 (2002), pp. 215–225.

[41] T. Söderlund, J.-M.I. Alakoskela, A.L. Pakkanen, and P.K.J. Kinnunen, *Comparison of the effects of surface tension and osmotic pressure on the interfacial hydration of a fluid phospholipid bilayer*, Biophys. J. 85 (2003), pp. 2333–2341.

[42] R.D. Lins, C.S. Pereira, and P.H. Hünenberger, *Trehalose–protein interactions in aqueous solution*, Proteins 55 (2004), pp. 177–186.

[43] G. Cottone, S. Giuffrida, G. Ciccotti, and L. Cordone, *Molecular dynamics simulation of sucrose- and trehalose-coated carboxy-myoglobin*, Proteins 59 (2005), pp. 291–302.

[44] G. Cottone, *A comparative study of carboxy myoglobin in saccharide–water systems by molecular dynamics simulation*, J. Phys. Chem. B 111 (2007), pp. 3563–3569.

[45] L. Cordone, G. Cottone, and S. Giuffrida, *Role of residual water hydrogen bonding in sugar/water/biomolecule systems: A possible explanation for trehalose peculiarity*, J. Phys. Condens. Matter 19 (2007), 205110.

[46] A. Lerbret, P. Bordat, F. Affouard, A. Hédoux, Y. Guinet, and M. Deschamps, *How do trehalose, maltose, and sucrose influence some structural and dynamical properties of lysozyme? Insight from molecular dynamics simulations*, J. Phys. Chem. B 111 (2007), pp. 9410–9420.

[47] A. Lerbret, F. Affouard, P. Bordat, A. Hédoux, Y. Guinet, and M. Deschamps, *Molecular dynamics simulations of lysozyme in water/sugar solutions*, Chem. Phys. 345 (2008), pp. 267–274.

[48] A.K. Sum, R. Faller, and J.J. de Pablo, *Molecular simulation study of phospholipid bilayers and insights of the interactions with disaccharides*, Biophys. J. 85 (2003), pp. 2830–2844.

[49] C.S. Pereira, R.D. Lins, I. Chandrasekhar, L.C.G. Freitas, and P.H. Hünenberger, *Interaction of the disaccharide trehalose with a phospholipid bilayer: A molecular dynamics study*, Biophys. J. 86 (2004), pp. 2273–2285.

[50] M.A. Villarreal, S.B. Diaz, E.A. Disalvo, and G.G. Montich, *Molecular dynamics simulation study of the interaction of trehalose with lipid membranes*, Langmuir 20 (2004), pp. 7844–7851.

[51] A. Skibinsky, R.M. Venable, and R.W. Pastor, *A molecular dynamics study of the response of lipid bilayers and monolayers to trehalose*, Biophys. J. 89 (2005), pp. 4111–4121.

[52] S. Leekumjorn and A.K. Sum, *Molecular investigation of the interactions of trehalose with lipid bilayers of DPPC, DPPE and their mixture*, Mol. Sim. 32 (2006), pp. 219–230.

[53] C.S. Pereira and P.H. Hünenberger, *Interaction of the sugars trehalose, maltose and glucose with a phospholipid bilayer: A comparative molecular dynamics study*, J. Phys. Chem. B 110 (2006), pp. 15572–15581.

[54] C.S. Pereira and P.H. Hünenberger, *The effect of trehalose on a phospholipid membrane under mechanical stress*, Biophys. J. 95 (2008), pp. 3525–3534.

[55] M. Lund, B. Jönsson, and C.E. Woodward, *Implications of a high dielectric constant in proteins*, J. Chem. Phys. 126 (2007), 225103.

[56] S. Ohki and K. Arnold, *Determination of liposome surface dielectric constant and hydrophobicity*, Methods Enzym. 367 (2003), pp. 253–272.

[57] R.M. Negri and D.L. Bernik, *Critical revision of apparent dielectric constants calculations in lipid–water interfaces*, J. Colloid Interface Sci. 226 (2000), pp. 364–366.

[58] I. Ueda and T. Yoshida, *Hydration of lipid membranes and the action mechanisms of anesthetics and alcohols*, Chem. Phys. Lipids 101 (1999), pp. 65–79.

[59] N.P. Franks, *Molecular targets underlying general anaesthesia*, Brit. J. Pharmacol. 147 (2006), pp. S72–S81.

[60] E.S. Rowe, *Lipid chain-length and temperature-dependence of ethanol phosphatidylcholine interactions*, Biochemistry 22 (1983), pp. 3299–3305.

[61] S.A. Simon and T.J. McIntosh, *Interdigitated hydrocarbon chain packing causes the biphasic transition behavior in lipid alcohol suspensions*, Biochim. Biophys. Acta 773 (1984), pp. 169–172.

[62] J.-S. Chiou, P.R. Krishna, H. Kamaya, and I. Ueda, *Alcohols dehydrate lipid membranes: An infrared study on hydrogen bonding*, Biochim. Biophys. Acta 1110 (1992), pp. 225–233.

[63] J.A. Barry and K. Gawrisch, *Direct NMR evidence for ethanol binding to the lipid–water interface of phospholipid bilayers*, Biochemistry 33 (1994), pp. 8082–8088.

[64] L.L. Loebbecke and G. Cevc, *Effects of short-chain alcohols on the phase behavior and interdigitation of phosphatidylcholine bilayer-membranes*, Biochim. Biophys. Acta 1237 (1995), pp. 59–69.

[65] L.L. Holte and K. Gawrisch, *Determining ethanol distribution in phospholipid multilayers with MAS–NOESY spectra*, Biochemistry 36 (1997), pp. 4669–4674.

[66] S.E. Feller, C.A. Brown, D.T. Nizza, and K. Gawrisch, *Nuclear Overhauser enhancement spectroscopy cross-relaxation rates and ethanol distribution across membranes*, Biophys. J. 82 (2002), pp. 1396–1404.

[67] H.V. Ly, D.E. Block, and M.L. Longo, *Interfacial tension effect of ethanol and lipid bilayer rigidity, stability, and area/molecules: A micropipette aspiration approach*, Langmuir 18 (2002), pp. 8988–8995.

[68] H.V. Ly and M.L. Longo, *The influence of short-chain alcohols on the interfacial tension, mechanical properties, area/molecules, and permeability of fluid lipid bilayers*, Biophys. J. 87 (2004), pp. 1013–1033.

[69] J. Chanda and S. Bandyopadhyay, *Distribution of ethanol in a model membrane: A computer simulation study*, Chem. Phys. Lett. 392 (2004), pp. 249–254.

[70] B.W. Lee, R. Faller, A.K. Sum, I. Vattulainen, M. Patra, and M. Karttunen, *Structural effects of small molecules on phospholipid bilayers investigated by molecular simulations*, Fluid Phase Equilib. 225 (2004), pp. 63–68.

[71] D. Pinisetty, D. Moldovan, and R. Devireddy, *The effect of methanol on lipid bilayers: An atomistic investigation*, Annu. Biomed. Eng. 34 (2006), pp. 1442–1451.

[72] M. Patra, E. Salonen, E. Terama, I. Vattulainen, R. Faller, B.W. Lee, J. Holopainen, and M. Karttunen, *Under the influence of alcohol: The effect of ethanol and methanol on lipid bilayers*, Biophys. J. 90 (2006), pp. 1121–1135.

[73] J. Chanda and S. Bandyopadhyay, *Perturbation of phospholipid bilayer properties by ethanol at a high concentration*, Langmuir 22 (2006), pp. 3775–3781.

[74] A.N. Dickey and R. Faller, *How alcohol chain-length and concentration modulate hydrogen bond formation in a lipid bilayer*, Biophys. J. 92 (2007), pp. 2366–2376.

[75] K. Ohki, K. Tamura, and I. Hatta, *Ethanol induces interdigitated gel phase (l-beta-i) between lamellar gel phase (l-beta') and ripple phase (p-beta') in phosphatidylcholine membranes – A scanning density meter study*, Biochim. Biophys. Acta 1028 (1990), pp. 215–222.

[76] J.X. Mou, J. Yang, C. Huang, and Z.F. Shao, *Alcohol induces interdigitated domains in unilamellar phosphatidylcholine bilayers*, Biochemistry 33 (1994), pp. 9981–9985.

[77] T.J. McIntosh, H.N. Lin, S.S. Li, and C.H. Huang, *The effect of ethanol on the phase transition temperature and the phase structure of monounsaturated phosphatidylcholines*, Biochim. Biophys. Acta 1510 (2001), pp. 219–230.

[78] P.W. Westerman, J.M. Pope, N. Phonphok, J.W. Doane, and D.W. Dubro, *The interaction of normal-alkanols with lipid bilayer membranes: A 2H-NMR study*, Biochim. Biophys. Acta 939 (1988), pp. 64–78.

[79] R.V. McDaniel, T.J. McIntosh, and S.A. Simon, *Non-electrolyte substitution for water in phosphatidylcholine bilayers*, Biochim. Biophys. Acta 731 (1983), pp. 97–108.

[80] W.P. Williams, P.J. Quinn, L.I. Tsonev, and R.D. Koynova, *The effects of glycerol on the phase-behavior of hydrated distearoylphosphatidylethanolamine and its possible relation to the mode of action of cryoprotectants*, Biochim. Biophys. Acta 1062 (1991), pp. 123–132.

[81] M. Yamazaki, M. Ohshika, N. Kashiwagi, and T. Asano, *Phase-transitions of phospholipid-vesicles under osmotic-stress and in the presence of ethylene–glycol*, Biophys. Chem. 43 (1992), pp. 29–37.

[82] M.J. Swamy and D. Marsh, *Thermodynamics of interdigitated phases of phosphatidylcholine in glycerol*, Biophys. J. 69 (1995), pp. 1402–1408.
[83] K. Nicolay, E.B. Smaal, and B. De Kruijff, *Ethylene–glycol causes acyl chain disordering in liquid-crystalline, unsaturated phospholipid model membranes, as measured by H-2 NMR*, FEBS Lett. 209 (1986), pp. 33–36.
[84] B. Bechinger, P.M. MacDonald, and J. Seelig, *Deuterium NMR-studies of the interactions of polyhydroxyl compounds and of glycolipids with lipid model membranes*, Biochim. Biophys. Acta 943 (1988), pp. 381–385.
[85] T.J. Anchordoguy, A.S. Rudolph, J. Carpenter, and J.H. Crowe, *Modes of interaction of cryoprotectant with membrane phospholipids during freezing*, Biophys. J. 51 (1987), p. A163.
[86] J.H. Crowe, J.F. Carpenter, L.M. Crowe, and T.J. Anchordoguy, *Are freezing and dehydration similar stress vectors – A comparison of modes of interaction of stabilizing solutes with biomolecules*, Cryobiology 27 (1990), pp. 219–231.
[87] P. Westh, *Unilamellar DMPC vesicles in aqueous glycerol: Preferential interactions and thermochemistry*, Biophys. J. 84 (2003), pp. 341–349.
[88] J. Faber-Barata and M. Sola-Penna, *Opposing effects of two osmolytes – trehalose and glycerol – on thermal inactivation of rabbit muscle 6-phosphofructo-1-kinase*, Mol. Cell. Biochem. 269 (2005), pp. 203–207.
[89] O. Vital de Oliveira, A. Farias de Moura, and L.C.G. Freitas, *A mechanism for the stabilization of the secondary structure of a peptide by liquid ethylene glycol and its aqueous solutions*, J. Mol. Struct. (Theochem) 808 (2007), pp. 93–96.
[90] A. Kyrychenko and T.S. Dyubko, *Molecular dynamics simulations of microstructure and mixing dynamics of cryoprotective solvents in water and in the presence of a lipid membrane*, Biophys. Chem. 136 (2008), pp. 23–31.
[91] N. Smolin and R. Winter, *Effect of temperature, pressure, and cosolvents on structural and dynamic properties of the hydration shell of SNase: A molecular dynamics computer simulation study*, J. Phys. Chem. B 112 (2008), pp. 997–1006.
[92] W.F. van Gunsteren, S.R. Billeter, A.A. Eising, P.H. Hünenberger, P. Krüger, A.E. Mark, W.R.P. Scott, and I.G. Tironi, *Biomolecular Simulation: The GROMOS96 Manual and User Guide*, vdf Hochschulverlag, ETH Zürich, Switzerland, 1996.
[93] W.R.P. Scott, P.H. Hünenberger, I.G. Tironi, A.E. Mark, S.R. Billeter, J. Fennen, A.E. Torda, T. Huber, P. Kruger, and W.F. van Gunsteren, *The GROMOS biomolecular simulation program package*, J. Phys. Chem. A 103 (1999), pp. 3596–3607.
[94] H.J.C. Berendsen, J.P.M. Postma, W.F. van Gunsteren, and J. Hermans, *Interaction models for water in relation to protein hydration*, in *Intermolecular Forces*, B. Pullman, ed., Reidel, Dordrecht, The Netherlands, 1981, pp. 331–342.
[95] R. Walser, A.E. Mark, W.F. van Gunsteren, M. Lauterbach, and G. Wipff, *The effect of force-field parameters on properties of liquids: Parametrization of a simple three-site model for methanol*, J. Chem. Phys. 112 (2000), pp. 10450–10459.
[96] D.P. Geerke and W.F. van Gunsteren, *The performance of non-polarizable and polarizable force-field parameter sets for ethylene glycol in molecular dynamics simulations of the pure liquid and its aqueous mixtures*, Mol. Phys. 105 (2007), pp. 1861–1881.
[97] R.D. Lins and P.H. Hünenberger, *A new GROMOS force field for hexopyranose-based carbohydrates*, J. Comput. Chem. 26 (2005), pp. 1400–1412.
[98] C. Oostenbrink, A. Villa, A.E. Mark, and W.F. Van Gunsteren, *A biomolecular force field based on the free enthalpy of hydration and solvation: The GROMOS force-field parameter sets 53A5 and 53A6*, J. Comput. Chem. 25 (2004), pp. 1656–1676.
[99] A. Glättli, X. Daura, and W.F. van Gunsteren, *Derivation of an improved simple point charge model for liquid water: SPC/A and SPC/L*, J. Chem. Phys. 116 (2002), pp. 9811–9828.
[100] H.B. Yu, D.P. Geerke, H.Y. Liu, and W.F. van Gunsteren, *Molecular dynamics simulations of liquid methanol and methanol–water mixtures with polarizable models*, J. Comput. Chem. 27 (2006), pp. 1494–1504.
[101] R.W. Hockney, *The potential calculation and some applications*, Methods Comput. Phys. 9 (1970), p. 136.
[102] H.J.C. Berendsen, J.P.M. Postma, W.F. van Gunsteren, A. DiNola, and J.R. Haak, *Molecular-dynamics with coupling to an external bath*, J. Chem. Phys. 81 (1984), pp. 3684–3690.
[103] J.P. Ryckaert, G. Ciccotti, and H.J.C. Berendsen, *Numerical-integration of Cartesian equations of motion of a system with constraints – Molecular-dynamics of n-alkanes*, J. Comput. Phys. 23 (1977), pp. 327–341.
[104] W.F. van Gunsteren and H.J.C. Berendsen, *Computer simulation of molecular dynamics: Methodology, applications and perspectives in chemistry*, Angew. Chem., Intl Ed. 29 (1990), pp. 992–1023.
[105] I.G. Tironi, R. Sperb, P.E. Smith, and W.F. van Gunsteren, *A generalized reaction field method for molecular-dynamics simulations*, J. Chem. Phys. 102 (1995), pp. 5451–5459.
[106] R.C. Weast (ed.), *Handbook of Chemistry and Physics*, CRC, Boca Raton, FL, 1976.
[107] G.H. Barbenza, *Dielectric dispersion in pure methyl alcohol as a function of temperature*, J. Chim. Phys.-Chim. Biol. 65 (1968), p. 906.
[108] J.A. Riddick, W.B. Bunger, and T.K. Sakano, *Organic Solvents, Physical Properties and Methods of Purification*, Wiley, New York, 1986.
[109] W.G.S. Scaife, *Effects of temperature and pressure on complex dielectric permittivity of liquid eugenol and glycerol*, J. Phys. D: Appl. Phys. 9 (1976), pp. 1489–1499.